8-6-2018

Tear Film Model Formulation: A 1-D Exploration

Emily Kiesel
esk4470@rit.edu

Tear Film Model Formulation: A 1-D Exploration

by

Emily Kiesel

A Thesis Submitted in Partial Fulfillment of the Requirements
for the Degree of Master of Science in Applied Mathematics
School of Mathematical Sciences, College of Science

Rochester Institute of Technology
Rochester, NY

August 6, 2018

Committee Approval:

Dr. Kara L. Maki — Date

School of Mathematical Sciences

Thesis Advisor

Dr. Nathaniel S. Barlow — Date

School of Mathematical Sciences

Committee Member

Dr. Matthew J. Hoffman — Date

School of Mathematical Sciences

Committee Member and Director of

Masters Program

Abstract

The study of the tear film of the eye is important for understanding the causes of dye eye syndrome, a disease causing damage to the ocular surface resulting in discomfort for many people. A popular mathematical model describing the evolution of the tear film thickness over time is a fourth-order nonlinear partial differential equation (PDE). This model has been formulated two different ways to facilitate numerical approximations. The first way is just one PDE including a fourth derivative along with the boundary and initial conditions that is solved for the tear film thickness. The second is a system of coupled second-order PDEs, with the analogous boundary and initial conditions, describing the tear film thickness and pressure. Typically, the second formulation is used when computing the solution as the first poses challenges. These challenges are generally attributed to approximating a scaled fourth derivative and specifying a third derivative for one of the boundary conditions.

In this thesis, I explore the computational differences between the two formulations of the tear film model in one spatial dimension. Both formulations are approximated by implementing a method of lines approach where spatial derivatives are approximated with second-order central finite differences, and then the system of differential equations are integrated forward in time using a backward Euler method. The stability of each numerical method is proven analytically with von Neumann analysis, and the usefulness of each formulation is characterized by studying the condition number of each discretization for different parameter values and boundary conditions. In particular, I examine the implications of the relationship between the lid function and boundary conditions. Lastly, a comparison is made with results from the two-dimensional equivalent model on a realistic blinking eye-shaped domain.

Contents

I. Introduction

The human eye is a complex organ, requiring a proper balance of water, lipids, mucins, protein, electrolytes, pH, and osmolarity on its ocular surface in order to function properly. A well performing tear film does a lot to protect the eye and allows for good vision [23]. It provides the optical surface needed for good refraction, counteracting imperfections in the cornea. The tear film also moistens the optical surface, keeping cells healthy and reducing friction with the eyelid. The proteins and mucins also protect the eye from irritants, debris, and infections as well as aid in cell repair. The tear film is crucial for eye health, as the epithelial cells do not have blood flow. It brings the epithelial cells metabolites, and transports carbon dioxide and metabolic waste away from the optical surface [7].

I.1 The tear film

The tear film has three principle components: a mucous layer, the aqueous "tear" layer, and the lipid layer. The mucous layer is at the tear film-eye interface and is between .2-.5μm thick. Secreted by goblet cells on the ocular surface, it aids in tear spread and protects the eye surface from pathogens [9]. Next is the aqueous layer. Made up of mostly water, it is between 2 μm and 10 μm thick [16]. This is primarily excreted by the lacrimal glands; however some water and electrolytes may come through the ocular surface. There is some debate as to whether the mucous and aqueous layers are actually distinct as it cannot be observed experimentally. Last, at the tear film-air interface is the lipid layer which is generally about .02-.05 μm thick [5]. This is primarily excreted by the meibomian glands, free sebaceous glands (oil secreting glands not associated with hair follicles) along the upper and lower lids [7].

During a blink, the lids redistribute the tear film. In between blinks, the tear film breaks up and dry spots emerge. Why this occurs is unknown [17]. Holly et al. proposed one hypothesis in which the lipid layer diffuses to the mucous layer creating areas of high hydrophobicity and accelerating tear film break up [13]. Another hypothesis is that tear film instability is caused by the breakup of the lipid layer accelerating tear film evaporation. A third hypothesis is that new underdeveloped corneal epithelial cells could initiate dry spot formation [10]. Whatever the cause, the tear film breaks up in between blinks and is reestablished during a blink.

To supply the tears, aqueous fluid comes in from the lacrimal glands, and drains into the puncta near the nose. There is also a flow of tears under the eye lid [19]. This provides lubrication for the

lid. As the eye opens, tear fluid from under the lid is revealed. On the exposed eye surface, most of the tear fluid resides in the menisci [21]. Mishima et al. estimate that 73% of the exposed tear film volume is located in these menisci [22]. Subsequently, an especially thin region, called the black line, forms adjacent to the meniscus due to meniscus-induced thinning [2].

The blinking mechanism is used to replenish the tear film and flush away debris. On average, a person blinks 15 times per minute [7]. Due to the difficulties of measuring such a thin film in a human subject without influencing the subject's blink patterns, experimental results vary; however, researchers have been able to get reasonable estimates of many aspects of a blink. For example, through high-speed photography Doane found that a blink normally lasts 0.258 seconds, where the downstroke of the upper lid lasts 0.082 and the upstroke lasts 0.176 seconds [8]. This suggests that the downstroke of a blink is twice as fast as the upstroke. Additionally, it is found to be common for a person to do a partial blink, where the eye doesn't completely close, rather than a complete blink [3].

However, not everyone's tear film does all of these things well. Those who suffer from dry-eye syndrome (DES) have an abnormal tear film; generally either there are not enough tears, or the tears are unusual. According to the Tear Film and Ocular Surface Society [6], "Dry eye is a multifactorial disease of the ocular surface characterized by a loss of homeostasis of the tear film, and accompanied by ocular symptoms, in which tear film instability and hyperosmolarity, ocular surface inflammation and damage, and neurosensory abnormalities play etiological roles." The main symptom is ocular discomfort. Without a properly functioning tear film, the eye is not fully protected from bacteria and may also suffer cellular damage [14]. In 2017, there were an estimated 5% to 50% of adults suffering from DES, so it is not a small problem, and the symptoms vary both in severity and condition [6]. A common treatment is artificial tears, however this is often inadequate. By developing models of the tear film, more can be learned about the specific causes of DES and treatments can be improved.

Many attempts at modeling the tear film have been made. The tear film is generally modeled as a thin film; thin, as the thickness of the tear film is much smaller than the length of the exposed optical surface, and flat, as the thickness is much smaller than the radius of curvature of the cornea [2]. This results in a fourth-order, nonlinear, partial differential equation (PDE) describing the evolution of the tear film thickness.

In order to analyze this model, researchers first considered a vertical slice of the eye. Braun reviews these one-dimensional modeling efforts [3]. In 2007, the one-dimensional model was

studied with flux boundary conditions and realistic lid motion by Heryudono et al. [12]. Due to numerical challenges, Heryudono et al. formulated the model as a system of PDEs with variables for tear film thickness and the flux on a blinking domain. This reduces the highest derivative to a third derivative. Approximating the system of PDEs using spectral methods, they were able to obtain results that were consistent with *in vivo* studies. Additionally, also using a thickness and flux model, Maki et al. were able to capture the effect of the black line region finite differences on an overset grid with a blinking domain [20]. In comparison to Heryudono et al., this work approximated spatial derivatives with curvilinear finite differences rather than spectral methods. Generally, due to the computational difficulties caused by having a fourth derivative, an alternate formulation is used that reduces the highest derivative used. However, this doubles the size of the problem, so it is somewhat unclear if the alternate formulation is really better.

The field progressed, and researchers began using two-dimensional models. At first, these models were on a fixed domain, neglecting the effects of the blink. Maki et al. developed ninth degree polynomials to dictate the eye-shaped domain [21]. A software called Overture (http://www.overtureframework.org/) developed by Henshaw was used to efficiently simulate the tear film dynamics. This work broke up the PDE into two equations with variables for the tear film thickness and the pressure [21]. Models like these lend themselves nicely to studying additional features of the tear film, such as osmolarity [18]. These works found the shape of the eye accelerating the mensicus-induced thinning in the canthi regions, as the curvature present causes low pressure and draws in the tear fluid. However, the effect of the blink on the tear film formation was not studied, and now researchers are trying to simulate the tear film evolution on an eye shaped, blink induced moving domain. How this effects the numerics of the problem is unclear.

As it is much less computationally expensive to try to learn from one-dimensional models than to try all simulations in two dimensions, to better inform the researchers working with the 2-D models, I seek to answer the following questions:

- Is there a meaningful difference between the single PDE model and the coupled PDE system with pressure?
- What are the aspects of the computation that cause the greatest effect on the conditioning of the numerics (i.e. lid motion, problem formulation, parameter choices, scalings, or boundary conditions)?
- Does the ability for the fluid to spread in two dimensions significantly alter the tear film

profile?

II. Model formulation

II.1 2-D model

First, I introduce the 2-D model. When modeling the aqueous layer, the tear fluid is assumed to be a thin, incompressible Newtonian fluid governed by the Navier-Stokes equations on the Cartesian coordinate system (x', y', z') with velocity (u', v', w') and pressure, p'. We nondimensionalize the equations as follows:

$$x = \frac{x'}{L^*},\ y = \frac{y'}{L^*},\ z = \frac{z'}{H},\ t = \frac{t'}{T},$$
$$u = \frac{u'}{\frac{L^*}{T}},\ v = \frac{v'}{\frac{L^*}{T}},\ w = \frac{w'}{\epsilon\frac{L^*}{T}},\ p = \frac{p'}{\frac{\mu T}{\epsilon^2}},$$

where the numerical values are given in Table 1 and $\epsilon = H/L^*$. Terms with $\epsilon = 1 \times 10^{-3}$ are considered small. For a thorough nondimensionalization see Braun [3].

Parameter	Value	Source
H	5×10^{-6} m	[21, 18]
L^*	5×10^{-3} m	[21, 18]
T	1.76×10^{-1} s	[8]
μ	1.3×10^{-3} N.s/m^2	[21, 18]
ρ	1×10^{3} kg/m^3	[21, 18]
σ	4.5×10^{-2} N/m	[21, 18]

Table 1: Dimensional parameters.

Applying lubrication theory, small terms are neglected, resulting with the leading order approximation below. Letting $h(x, y, t)$ represent the tear film thickness, inside the tear film $(0 < z < h)$, the equation governing the conservation of mass is:

$$\partial_x u + \partial_y v + \partial_z w = 0.$$

To conserve momentum, in the x, y, z directions we have,

$$-\partial_x p + \partial_z^2 u = 0, -\partial_y p + \partial_z^2 v = 0, -\partial_z p = 0$$

respectively. At the tear film-ocular surface interface $(z = 0)$, we have the no-slip and no penetration conditions $u = v = w = 0$. At the tear film air interface $(z = h)$, we assume zero tangential stresses $\partial_z v = \partial_z u = 0$. Lastly, to balance the normal stress with the pressure, we have $p - p_a = -S\Delta h$, where p_a is atmospheric pressure, and $S = \frac{\epsilon^3 \sigma}{\mu U_0}$ is the inverse capillary number, which gives the ratio of surface tension to viscous forces [18].

These equations can be combined into one evolution equation of the form

$$h_t + \nabla \cdot \mathbf{Q} = \mathbf{0}, \tag{II.1}$$

where $\mathbf{Q}$ is the fluid flux [21]. In terms of tear thickness, we have

$$\mathbf{Q} = \frac{Sh^3}{3} \nabla \Delta h.$$

To help with the computation, as done in Maki et al. [21], we can write equation (II.1) as the system:

$$h_t - \nabla \cdot \left(\frac{h^3}{3} \nabla p \right) = 0,$$
$$p + S\Delta h = 0.$$

Note that here p refers to the difference from atmospheric pressure. If $p = 0$, then the internal fluid pressures were equal to atmospheric pressure.

This system can be paired with a variety of four boundary conditions and an initial condition, which will be elaborated upon in a further subsection.

II.2 1-D model

In order to learn about the numerical behavior of the 2-D model, a 1-D model was used. To do this, we consider one vertical slice of the eye, so the thickness is given by $h(x, t)$ for $t > 0$ and $0 < x < L(t)$, where $L(t)$ is the position of the upper lid and characterized in the next section, so that the governing evolution equation is given by

$$\frac{\partial h}{\partial t} + \frac{\partial}{\partial x} \left(S \frac{h^3}{3} \frac{\partial^3 h}{\partial x^3} \right) = 0.$$

We fix the tear film thickness at the lower and upper boundaries, $h(0, t) = h(L(t), t) = h_0$, where $h_0 = 13$ is chosen to match experimental measurements of the tear meniscus width of 65 μm [11].

This boundary condition will be used in all simulations throughout the thesis. For the second boundary condition applied at the upper and lower lids, we either control the influx/efflux of tear fluid or we specify the pressure. In this section, we present the no-flux boundary conditions. Later we will explore how the boundary conditions affect the conditioning of the numerical approximation. In the no-flux boundary condition, we allow no fluid to enter or leave the eye at the lower lid by enforcing a zero flux condition given by

$$S\frac{h(0,t)^3}{3}\frac{\partial^3 h}{\partial x^3}(0,t) = 0$$

To derive the no flux boundary condition at the upper lid, we determine what it must be in order to conserve volume. Using the fact that the tear film volume can be found by integrating the tear film thickness along the opening of the eye, the boundary condition is derived below:

$$\begin{aligned} V(t) &= \int_0^{L(t)} h(x,t)dx, \\ \frac{dV}{dt} &= \int_0^{L(t)} \frac{\partial h}{\partial t}(x,t)dx + h_0\dot{L}(t). \end{aligned}$$

Notice that the integrand is the first term of the PDE. Substituting the remaining terms in yields:

$$\begin{aligned} \frac{dV}{dt} &= \int_0^{L(t)} -\frac{\partial}{\partial x}\left(S\frac{h^3}{3}\frac{\partial^3 h}{\partial x^3}\right)dx + h_0\dot{L}(t) \\ \frac{dV}{dt} &= \left(-S\frac{h^3}{3}\frac{\partial^3 h}{\partial x^3}\right)\Big|_0^{L(t)} + h_0\dot{L} = -\left(S\frac{h^3}{3}\frac{\partial^3 h}{\partial x^3}\right)\Big|_{x=L(t)} + \left(S\frac{h^3}{3}\frac{\partial^3 h}{\partial x^3}\right)\Big|_{x=0} + h_0\dot{L}. \end{aligned}$$

However, since the volume is constant and we are not allowing any fluid flux at the lower lid, this becomes:

$$\begin{aligned} 0 &= -\left(S\frac{h^3}{3}\frac{\partial^3 h}{\partial x^3}\right)\Big|_{x=L(t)} + h_0\dot{L}, \\ \left(S\frac{h^3}{3}\frac{\partial^3 h}{\partial x^3}\right)\Big|_{x=L(t)} &= h_0\dot{L}. \end{aligned}$$

Since this formulation of the PDE has a fourth derivative, its spatial derivatives cannot be approximated using built in functions in Overture. Therefore, a model involving pressure is used. We define the pressure to be a function of x and t, namely $p(x,t) = -S\frac{\partial^2 h}{\partial x^2}$. The boundary value

problem in terms of h and p is

$$\begin{aligned} \frac{\partial h}{\partial t} - \frac{\partial}{\partial x}\left(\frac{h^3}{3}\frac{\partial p}{\partial x}\right) &= 0, \\ p + S\frac{\partial^2 h}{\partial x^2} &= 0, \\ h(0,t) = h(L(t),t) &= h_0, \\ \left(\frac{h^3}{3}\frac{\partial p}{\partial x}\right)\Big|_{x=0} = 0, \quad \left(\frac{h^3}{3}\frac{\partial p}{\partial x}\right)\Big|_{x=L(t)} &= -h_0\dot{L}(t). \end{aligned}$$

Initial conditions will be discussed in section II.4. Notice that the flux boundary condition changes sign as p contains a negative.

For ease of computation, we mapped the moving domain into a fixed domain using the following change of coordinates $\xi = \frac{x}{L(t)}$ so that $h(x,t) = \hat{h}(\xi(x,t),t)$. The evolution on the fixed domain then becomes:

$$\begin{aligned} \frac{\partial \hat{h}}{\partial t} - \frac{\xi \dot{L}}{L}\frac{\partial \hat{h}}{\partial \xi} - \frac{1}{L^2}\frac{\partial}{\partial \xi}\left(\frac{\hat{h}^3}{3}\frac{\partial \hat{p}}{\partial \xi}\right) &= 0, \\ \hat{p} + \frac{S}{L^2}\frac{\partial^2 \hat{h}}{\partial \xi^2} &= 0, \end{aligned}$$

with corresponding boundary conditions given by

$$\begin{aligned} \hat{h}(0,t) = \hat{h}(1,t) &= h_0, \\ \left(\frac{\hat{h}^3}{3L}\frac{\partial \hat{p}}{\partial \xi}\right)\Big|_{\xi=0} = 0, \quad \left(\frac{\hat{h}^3}{3L}\frac{\partial \hat{p}}{\partial \xi}\right)\Big|_{\xi=1} &= -h_0\dot{L}(t). \end{aligned}$$

As before, the volume is conserved with the condition at the upper lid:

$$0 = h_0\dot{L} - \frac{\hat{h}(1,t)^3}{3L}\frac{\partial \hat{p}}{\partial \xi}(1,t)$$

$$\frac{\hat{h}(1,t)^3}{3L}\frac{\partial \hat{p}}{\partial \xi}(1,t) = -h_0\dot{L}.$$

II.3 Boundary conditions

There were three different sets of boundary conditions used. I will describe them for the single PDE. The first is a condition on the flux that conserves tear fluid volume. Symbolically,

Boundary Conditions 1:

$$\begin{aligned} \hat{h}(0,t) &= h_0, \\ \hat{h}(1,t) &= h_0, \\ \left(\frac{S\hat{h}^3}{3L^3}\frac{\partial^3\hat{h}}{\partial\hat{\xi}^3}\right)\Big|_{\hat{\xi}=0} &= 0, \\ \left(\frac{S\hat{h}^3}{3L^3}\frac{\partial^3\hat{h}}{\partial\hat{\xi}^3}\right)\Big|_{\hat{\xi}=1} &= h_0\dot{L}(t). \end{aligned}$$

The second is a similar condition, however tear fluid is not conserved. Instead, it relieves some of the pressure at the upper lid. I assume a tear film of thickness h_e exists under the upper lid and is exposed as the lid opens [15].

Boundary Conditions 2:

$$\begin{aligned} \hat{h}(0,t) &= h_0, \\ \hat{h}(1,t) &= h_0, \\ \left(\frac{S\hat{h}^3}{3L^3}\frac{\partial^3\hat{h}}{\partial\hat{\xi}^3}\right)\Big|_{\hat{\xi}=0} &= 0, \\ \left(\frac{S\hat{h}^3}{3L^3}\frac{\partial^3\hat{h}}{\partial\hat{\xi}^3}\right)\Big|_{\hat{\xi}=1} &= (h_0 - h_e)\dot{L}(t). \end{aligned}$$

The third is fixing the pressure at the lower and upper lids. This was derived from the initial condition I derived above. For the regular system these are:

Boundary Conditions 3:

$$\begin{aligned} \hat{h}(0,t) &= h_0, \\ \hat{h}(1,t) &= h_0, \\ \frac{1}{L^2}\frac{\partial^2\hat{h}}{\partial\hat{\xi}^2}(0,t) &= 2, \\ \frac{1}{L^2}\frac{\partial^2\hat{h}}{\partial\hat{\xi}^2}(1,t) &= \frac{3\dot{L}}{2Sh_0^2} + 2. \end{aligned}$$

For the pressure system, we use the fact that $\hat{p} = -S\frac{1}{L^2}\frac{\partial^2\hat{h}}{\partial\hat{\xi}^2}$ to rewrite the last two boundary

conditions in terms of the pressure. Symbolically,

Boundary Conditions 1:

$$\begin{aligned}\hat{h}(0,t) &= h_0,\\ \hat{h}(1,t) &= h_0,\\ \left(\frac{\hat{h}^3}{3L}\frac{\partial \hat{p}}{\partial \xi}\right)\Big|_{\xi=0} &= 0,\\ \left(\frac{\hat{h}^3}{3L}\frac{\partial \hat{p}}{\partial \xi}\right)\Big|_{\xi=1} &= -h_0\dot{L}(t),\end{aligned}$$

Boundary Conditions 2:

$$\begin{aligned}\hat{h}(0,t) &= h_0,\\ \hat{h}(1,t) &= h_0,\\ \left(\frac{\hat{h}^3}{3L}\frac{\partial \hat{p}}{\partial \xi}\right)\Big|_{\xi=0} &= 0,\\ \left(\frac{\hat{h}^3}{3L}\frac{\partial \hat{p}}{\partial \xi}\right)\Big|_{\xi=1} &= -(h_0-h_e)\dot{L}(t),\end{aligned}$$

Boundary Conditions 3:

$$\begin{aligned}\hat{h}(0,t) &= h_0,\\ \hat{h}(1,t) &= h_0,\\ \hat{p}(0,t) &= -2S,\\ \hat{p}(1,t) &= \frac{-3\dot{L}}{2h_0^2} - 2S.\end{aligned}$$

II.4 Initial conditions

I used two different initial conditions. In the single PDE case, I have an initial condition on the thickness, $\hat{h}$, and in the coupled system, I have initial conditions on both the thickness $\hat{h}$ and the pressure $\hat{p}$. The first initial condition is a quartic equation built to have a parabolic shape and satisfy all the boundary conditions. Specifically, I found parameters a, b, c, d, and e in $\hat{h}(\xi,0) = a\xi^4 + b\xi^3 + c\xi^2 + d\xi + e$ by satisfying $\hat{h}(0,0) = h_0$, $\hat{h}(1,0) = h_0$, $\frac{\partial^3 \hat{h}}{\partial \xi^3}(0,0) = 0$, and $\frac{\partial^3 \hat{h}}{\partial \xi^3}(1,0) = \frac{3\dot{L}L^3}{Sh_0^2}$.

The result was the following equation with the free variable c

$$\hat{h}(\xi,0) = \frac{\dot{L}L^3}{8h_0^2 S}\xi^4 + c\xi^2 + \left(-c - \frac{\dot{L}L^3}{8h_0^2 S}\right)\xi + h_0.$$

We chose $c = 1$ to include the quadratic term. Thus, the initial condition used was

$$\hat{h}(\xi,0) = \frac{\dot{L}L^3}{8h_0^2 S}\xi^4 + \xi^2 + \left(-1 - \frac{\dot{L}L^3}{8h_0^2 S}\right)\xi + h_0,$$
$$\hat{p}(\xi,0) = \frac{-3\dot{L}L}{2h_0^2}\xi^2 - \frac{2S}{L^2}.$$

The second initial condition was adapted from Braun and King-Smith [4]. While having a similar shape, this initial thickness profile is much thinner in the middle and has more variation in initial pressure.

$$\hat{h}(\xi,0) = 1 + (h_0 - 1)(2\xi - 1)^4,$$
$$\hat{p}(\xi,0) = -\frac{48S}{L^2}(h_0 - 1)(2\xi - 1)^2.$$

Figures 1 and 2 show both sets of initial conditions.

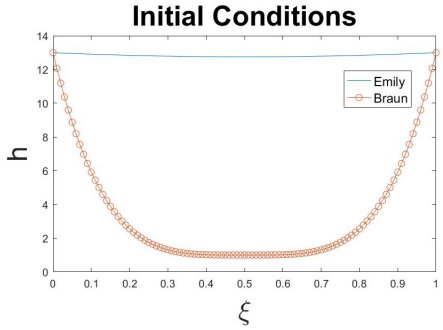

Figure 1: Initial tear film thicknesses.

II.5 Blink approximation

Three different functions, $L(t)$, were used to approximate the position of the upper lid over the time of a blink. First, a simple trigonometric function, then an exponential function fit to data, and lastly, a bivariate Fourier series approximation of the lid margin found by a least-square approximation of data from a partial blink.

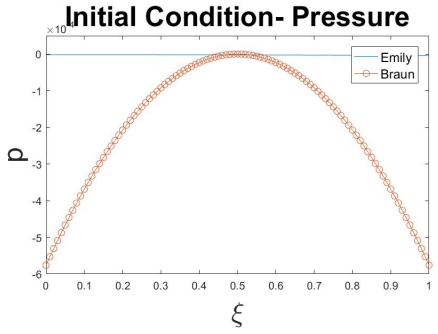

Figure 2: Initial pressures.

The "toy" model of the eyelid motion was the trigonometric equation. It exemplifies the primary characteristics of the lid: bounded, periodic, and completes a blink in finite time. The derivative which dictates the lid velocity is also bounded and periodic. It is also easy to manipulate the period and range for exploratory purposes. The function used was

$$L(t) = \begin{cases} .8\sin^2(\gamma t) + .2 & 0 < t \leq 1 \\ .8\cos^2(\gamma(t-1)) + .2 & 1 < t < 1.5 \end{cases}, \tag{II.2}$$

with lid speed given by

$$\dot{L}(t) = \begin{cases} 1.6\gamma\cos(\gamma t)\sin(\gamma t) & 0 < t \leq 1 \\ -1.6\gamma\cos(\gamma(t-1))\sin(\gamma(t-1)) & 1 < t < 1.5 \end{cases}. \tag{II.3}$$

This trigonometric equation was selected so that the range was from 0.2 to 1 to simulate a partial blink and the eye starts in its most closed position. The parameter γ can be varied to simulate different lid speeds. For our nondimensionalization, I chose $\gamma = \pi$ so that it takes 1 nondimensional time unit for the eye to open and takes .5 nondimensional time units to close as shown in Figure 3. If $\gamma = 0$, then the lid does not move.

Moving forward in complexity, the second lid function used was developed by Aydemir et al. [1]. This function also exemplifies the primary characteristics of eyelid motion, including the large initial acceleration of the lid. Motivated by that, they started with a function for the velocity of the lid of the form:

$$U(t) = \begin{cases} \frac{TU_0}{L*}\left(\lambda\sqrt{\frac{Tt}{\tau}}e^{-\frac{Tt}{\tau}} - \frac{Tt}{\tau}\right) & 0 \leq Tt \leq t^* \\ 0 & t^\star \leq Tt \end{cases},$$

where L^* and T are defined in Table 1.

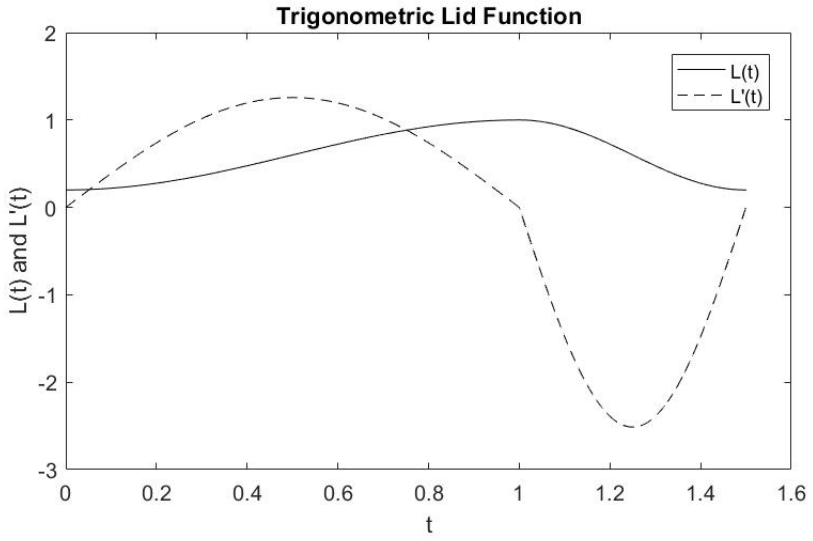

Figure 3: The periodic lid and lid velocity functions for given by equations (II.2) and (II.3) for $\gamma = \pi$.

Then, this model was fit to data found by Wong to obtain parameter values $U_0 = 0.0163$ m/s, $\tau = 0.0865$ s, $\lambda = 11.6$, and $t^* = 0.180$ s [24]. Solving the initial value problem

$$\frac{dL}{dt} = U(t), \quad L(0) = L_{cl},$$

where L_{cl} is the closed position of the upper lid, they found the equation to describe the lid motion:

$$L(t) = \frac{L_{cl}}{L^*} + \frac{TU_0}{L^*}\tau\left(-\frac{1}{2}\left[\frac{Tt}{\tau}\right]^2 + \lambda\left[\frac{\sqrt{\pi}}{2}\text{erf}\left(\sqrt{\frac{Tt}{\tau}}\right) - \sqrt{\frac{Tt}{\tau}}e^{-\frac{Tt}{\tau}}\right]\right).$$

They chose $L_{cl} = .002$ m to be consistent with the length of the exposed eye surface during a partial blink. Figure 4 shows the lid position and speed where you can see the rapid acceleration of the upper lid at the beginning of the upstroke and rapid deceleration at the end of the down stroke.

Finally, the most realistic lid function used was developed by Dylan Chapp under the advisement of Dr. Rich Braun and Dr. Toby Driscoll from the Department of Mathematical Sciences at the University of Delaware. At its core, it is a double Fourier series in space and time created using data from a video of a person performing a partial blink. It is a 2-D function, so in order to use it for the 1-D model, I focused on the center of the exposed eye surface. I found the the position of the lower lid at the point closest to the center of the exposed eye and subtracted it from the upper lid position closest to the center of the exposed eye. From this, we know how much of the eye is exposed at that point at each point in time. This was then rescaled so that at time zero, the lid is

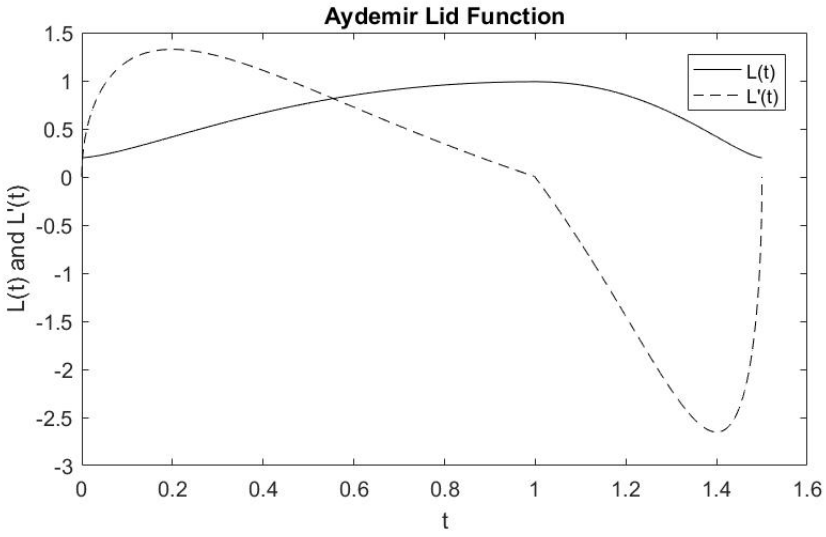

Figure 4: The lid and lid velocity functions based on work of Aydemir et al. [1].

at its most closed, namely $L(0) = .2$, and attains its maximum of 1 at time 1, L(1)=1 so as to satisfy our non-dimensionalization. Figure 5 displays the lid position and speed from a subject's partial blink. The realistic blink speed is more variable and faster on the downstroke, but shares the same features as the other lid motion.

III. Numerical computation

Discussion will focus on the non-linear PDE on a mapped domain and the PDE system on a mapped domain as they solve the same problem but are formatted differently. Both boundary value problems are discretized on a Cartesian grid, using a method of lines approach. First, we discretized spatial derivatives using second-order central finite differences. To mimic the way the PDE is approximated in Overture, I did not use MATLAB's built in solvers to integrate the system of ordinary differential equations with time as was done in previous works [12, 21]. Instead, I used a first-order backward difference formula to integrate the system forward in time. Consequently, at each time step, I must approximate the root of a nonlinear system of equations. Therefore, I wrote up all parts of the Newton solver myself. This allowed greater flexibility in exploring the effect of changing parameters and boundary conditions, and is more comparable to how the equations are generally solved in the 2-D case.

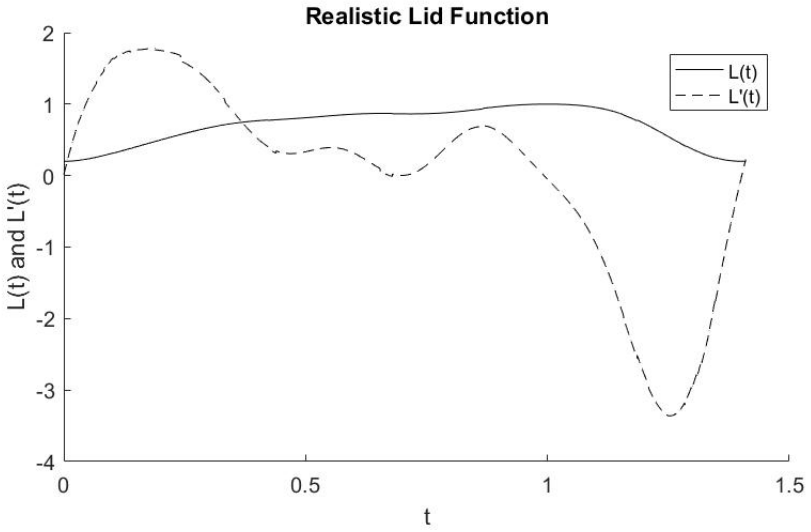

Figure 5: The lid and lid velocity functions fit to images of a subject performing a partial blink.

III.1 Single PDE

For the case of the single non-linear PDE with moving boundary, I present the numerical scheme used. First, I discretized the fixed spatial domain uniformly with $\xi_j = j\Delta\xi$, for $j = -2, \ldots, m+2$, where $m = 1/\Delta\xi$. I have introduced two ghost points at each end of the domain to facilitate the approximation of the boundary conditions. Time is discretized by $t^n = n\Delta t$. The numerical scheme approximates the tear film thickness at each spatial grid location and discrete time, $h_j^n \approx h(\xi_j, t^n)$.

At each time step, Newton's method is implemented to find the root of vector-valued function $\mathbf{F}(\mathbf{h}, \mathbf{t})$ from $\mathbb{R}^{m+5}$ to $\mathbb{R}^{m+5}$. Specifically, the components of $\mathbf{F}$ evaluated at time t^{n+1} is given

by

$$F_{j+2}^{n+1} = \begin{cases} \frac{S}{6L^3(\Delta\xi)^3}\left(\hat{h}_0^{n+1}\right)^3\left(\hat{h}_2^{n+1} - 2\hat{h}_1^{n+1} + 2\hat{h}_{-1}^{n+1} - \hat{h}_{-2}^{n+1}\right), & \text{for } j = -2 \\ \hat{h}_0^{n+1} - \hat{h}_0^n + \frac{S\Delta t}{3L^4(\Delta\xi)^4}\left(\hat{h}_0^{n+1}\right)^3\left(\hat{h}_2^{n+1} - 4\hat{h}_1^{n+1} + 6\hat{h}_0^{n+1} - 4\hat{h}_{-1}^{n+1} + \hat{h}_{-2}^{n+1}\right) & \\ \quad + \frac{S\Delta t}{2L^4(\Delta\xi)^4}\left(\hat{h}_0^{n+1}\right)^2\left(\hat{h}_1^{n+1} - \hat{h}_{-1}^{n+1}\right)\left(\frac{1}{2}\hat{h}_2^{n+1} - \hat{h}_1^{n+1} + \hat{h}_{-1}^{n+1} - \frac{1}{2}\hat{h}_{-2}^{n+1}\right), & \text{for } j = -1 \\ \hat{h}_0^{n+1} - h_0, & \text{for } j = 0 \\ \hat{h}_j^{n+1} - \hat{h}_j^n - \frac{\dot{L}\Delta t\xi_j}{2L\Delta\xi}\left(\hat{h}_{j+1}^{n+1} - \hat{h}_{j-1}^{n+1}\right) & \\ \quad + \frac{S\Delta t}{3L^4(\Delta\xi)^4}\left(\hat{h}_j^{n+1}\right)^3\left(\hat{h}_{j+2}^{n+1} - 4\hat{h}_{j+1}^{n+1} + 6\hat{h}_j^{n+1} - 4\hat{h}_{j-1}^{n+1} + \hat{h}_{j-2}^{n+1}\right) & \text{for } j = 1, \ldots, m-1 \\ \quad + \frac{S\Delta t}{2L^4(\Delta\xi)^4}\left(\hat{h}_j^{n+1}\right)^2\left(\hat{h}_{j+1}^{n+1} - \hat{h}_{j-1}^{n+1}\right)\left(\frac{1}{2}\hat{h}_{j+2}^{n+1} - \hat{h}_{j+1}^{n+1} + \hat{h}_{j-1}^{n+1} - \frac{1}{2}\hat{h}_{j-2}^{n+1}\right), & \\ \hat{h}_m^{n+1} - h_0, & \text{for } j = m \\ \hat{h}_m^{n+1} - \hat{h}_m^n - \frac{\dot{L}\Delta t\xi_m}{2L\Delta\xi}\left(\hat{h}_{m+1}^{n+1} - \hat{h}_{m-1}^{n+1}\right) & \\ \quad + \frac{S\Delta t}{3L^4(\Delta\xi)^4}\left(\hat{h}_m^{n+1}\right)^3\left(\hat{h}_{m+2}^{n+1} - 4\hat{h}_{m+1}^{n+1} + 6\hat{h}_m^{n+1} - 4\hat{h}_{m-1}^{n+1} + \hat{h}_{m-2}^{n+1}\right) & \text{for } j = m+1 \\ \quad + \frac{S\Delta t}{2L^4(\Delta\xi)^4}\left(\hat{h}_m^{n+1}\right)^2\left(\hat{h}_{m+1}^{n+1} - \hat{h}_{m-1}^{n+1}\right)\left(\frac{1}{2}\hat{h}_{m+2}^{n+1} - \hat{h}_{m+1}^{n+1} + \hat{h}_{m-1}^{n+1} - \frac{1}{2}\hat{h}_{m-2}^{n+1}\right), & \\ \frac{S}{6L^3(\Delta\xi)^3}\left(\hat{h}_m^{n+1}\right)^3\left(\hat{h}_{m+2}^{n+1} - 2\hat{h}_{m+1}^{n+1} + 2\hat{h}_{m-1}^{n+1} - \hat{h}_{m-2}^{n+1}\right) - h_0\dot{L} & \text{for } j = m+2 \end{cases}.$$

To approximate the third derivative at the boundary (see components F_0^{n+1} defined by $j = -2$ and F_{m+4}^{n+1} defined by $j = m+2$), I need two grid points on each side of the boundary grid point. This is why I introduced two ghost points at both boundaries. Thus, I have $m+5$ variables to solve for and I need an two additional equations to determine the tear film thickness at the ghost points. The first equation is the flux boundary condition itself. For the second equation, I evaluated the PDE at the boundary (see components $j = -1$ and $j = m+1$). Finally, the dirichlet boundary conditions are enforced in components $j = 0$ and $j = m$.

At the i-th Newton iteration, the solver is set up to solve $J(\hat{\mathbf{h}}_i)(\hat{\mathbf{h}}_i - \hat{\mathbf{h}}^n) = -\mathbf{F}(\hat{\mathbf{h}}_i)$, where $J \in \mathbb{R}^{(m+5)\times(m+5)}$ is the Jacobian of $\mathbf{F}$, and $\hat{\mathbf{h}}_i$ is i-th approximation of the root $\hat{\mathbf{h}}^{n+1}$. The components

of the Jacobian are given by

$$J_{i+2,j+2} = \begin{cases} 1, & \text{for } i = 0, m,\ j = i, \\ -\frac{S}{6L^3}\left(\hat{h}_0^{n+1}\right)^3, & \text{for } i = -1, j = -1, \\ -\frac{S}{6L^3}\left(\hat{h}_0^{n+1}\right)^3, & \text{for } i = m+5, \text{ and } j = m+1, \\ \frac{S}{3L^3}\left(\hat{h}_0^{n+1}\right)^3, & \text{for } i = 1 \text{ and } j = 2, \\ \frac{S}{3L^3}\left(\hat{h}_0^{n+1}\right)^3, & \text{for } i = m+5 \text{ and } j = m+2, \\ -\frac{S}{2L^3}\left(\hat{h}_0^{n+1}\right)^2\left(\hat{h}_2^{n+1} - 2\hat{h}_1^{n+1} + 2\hat{h}_{-1}^{n+1} - \hat{h}_{-2}^{n+1}\right), & \text{for } i = 1 \text{ and } j = 3, \\ -\frac{S}{2L^3}\left(\hat{h}_0^{n+1}\right)^2\left(\hat{h}_2^{n+1} - 2\hat{h}_1^{n+1} + 2\hat{h}_{-1}^{n+1} - \hat{h}_{-2}^{n+1}\right), & \text{for } i = m+5 \text{ and } j = m+3, \\ \frac{S}{3L^3}\left(\hat{h}_0^{n+1}\right)^3, & \text{for } i = 1 \text{ and } j = 4, \\ \frac{S}{3L^3}\left(\hat{h}_0^{n+1}\right)^3, & \text{for } i = m+5 \text{ and } j = m+4, \\ -\frac{S}{6L^3}\left(\hat{h}_0^{n+1}\right)^3, & \text{for } i = 1 \text{ and } j = 5, \\ -\frac{S}{6L^3}\left(\hat{h}_0^{n+1}\right)^3, & \text{for } i = m+5 \text{ and } j = m+5, \\ \frac{S\Delta t}{3L^4(\Delta\xi)^4}\left(\hat{h}_j^{n+1}\right)^3 - \frac{S\Delta t}{4L^4(\Delta\xi)^4}\left(\hat{h}_j^{n+1}\right)^2\left(\hat{h}_{j+1}^{n+1} - \hat{h}_{j-1}^{n+1}\right), & \text{for } i = 3, \ldots, m+2 \text{ and } j = i-2, \\ \dfrac{\xi_j \dot{L}\Delta t}{2\Delta\xi L} - \dfrac{4S\Delta t}{3L^4\Delta\xi^4}\left(\hat{h}_j^{n+1}\right)^3 + \\ \dfrac{S\Delta t}{2L^4\Delta\xi^4}\left(\hat{h}_j^{n+1}\right)^2\left(-\dfrac{1}{2}\hat{h}_{j+2}^{n+1} + 2\hat{h}_{j+1}^{n+1} - 2\hat{h}_{j-1}^{n+1} + \dfrac{1}{2}\hat{h}_{j+2}^{n+1}\right), & \text{for } i = 3, \ldots, m+2 \text{ and } j = i-1, \\ 1 + \dfrac{S\Delta t}{L^4\Delta\xi^4}\left(\hat{h}_j^{n+1}\right)^2\left(\hat{h}_{j+2}^{n+1} - 4\hat{h}_{j+1}^{n+1} + 8\hat{h}_j^{n+1} - 4\hat{h}_{j-1}^{n+1} + \hat{h}_{j-2}^{n+1}\right) \\ + \dfrac{S\Delta t}{L^4\Delta\xi^4}\hat{h}_j^{n+1}\left(\hat{h}_{j+1}^{n+1} - \hat{h}_{j-1}^{n+1}\right)\left(\dfrac{1}{2}\hat{h}_{j+2}^{n+1} - \hat{h}_{j+1}^{n+1} + \hat{h}_{j-1}^{n+1} - \dfrac{1}{2}\hat{h}_{j-2}^{n+1}\right), & \text{for } i = 3, \ldots, m+2 \text{ and } j = i, \\ -\dfrac{\xi_j \dot{L}\Delta t}{2\Delta\xi L} - \dfrac{4S\Delta t}{3L^4\Delta\xi^4}\left(\hat{h}_j^{n+1}\right)^3 \\ + \dfrac{S\Delta t}{2L^4\Delta\xi^4}\left(\hat{h}_j^{n+1}\right)^2\left(\dfrac{1}{2}\hat{h}_{j+2}^{n+1} - 2\hat{h}_{j+1}^{n+1} + 2\hat{h}_{j-1}^{n+1} - \dfrac{1}{2}\hat{h}_{j+2}^{n+1}\right), & \text{for } i = 3, \ldots, m+2 \text{ and } j = i+1, \\ \frac{S\Delta t}{3L^4(\Delta\xi)^4}\left(\hat{h}_j^{n+1}\right)^3 + \frac{S\Delta t}{4L^4(\Delta\xi)^4}\left(\hat{h}_j^{n+1}\right)^2\left(\hat{h}_{j+1}^{n+1} - \hat{h}_{j-1}^{n+1}\right), & \text{for } i = 3, \ldots, m+2, \text{and } j = i+2, \\ 0, & \text{otherwise} \end{cases}.$$

III.2 Coupled PDE

For the case of the coupled non-linear PDEs on a mapped domain, now, I discretized the fixed spatial domain uniformly with $\xi_j = j\Delta\xi$, for $j = -1, \ldots, m+1$, where $m = 1/\Delta\xi$. Time is discretized by $t^n = n\Delta t$. Again, the numerical scheme approximates the tear film thickness and the pressure at each spatial grid location and discrete time, $\hat{h}_j^n \approx \hat{h}(\xi_j, t^n)$ and $\hat{p}_j^n \approx \hat{p}(\xi_j, t^n)$,

respectively. I have introduced one ghost point at each end of the domain to facilitate the approximation of the boundary conditions. At each time step, Newton's method is implemented to find the root of vector-valued function $\mathbf{E}(\hat{\mathbf{h}}, \hat{\mathbf{p}})$ from $\mathbb{R}^{2m+6}$ to $\mathbb{R}^{2m+6}$. Specifically, the components of $\mathbf{E}$ evaluated at time t^{n+1} is given by

$$E_{j+1}^{n+1} = \begin{cases} \hat{h}_0^{n+1} - h_0, & \text{for } j = -1, \\ \dfrac{\hat{h}_j^{n+1} - \hat{h}_j^n}{\Delta t} - \dfrac{\xi_j \dot{L}}{L}\left(\dfrac{\hat{h}_{j+1}^{n+1} - \hat{h}_{j-1}^{n+1}}{2\Delta\xi}\right) - \\ \quad \dfrac{\left(\hat{h}_j^{n+1}\right)^2}{L^2}\left(\dfrac{\hat{p}_{j+1}^{n+1} - \hat{p}_{j-1}^{n+1}}{2\Delta\xi}\right)\left(\dfrac{\hat{h}_{j+1}^{n+1} - \hat{h}_{j-1}^{n+1}}{2\Delta\xi}\right) - \dfrac{\left(\hat{h}_j^{n+1}\right)^3}{3L^2}\dfrac{\hat{p}_{j+1}^{n+1} - 2\hat{p}_j^{n+1} + \hat{p}_{j-1}^{n+1}}{\Delta\xi^2} & \text{for } j = 0, \ldots, m, \\ \hat{h}_{m+1}^{n+1} - h_0, & \text{for } j = m+1, \\ \frac{1}{6L\Delta\xi}\left(\hat{h}_0^{n+1}\right)^3\left(\hat{p}_1^{n+1} - \hat{p}_{-1}^{n+1}\right), & \text{for } j = m+2, \\ \hat{p}_{j-(m+3)}^{n+1} + \frac{S}{L^2}\left(\frac{\hat{h}_{j+1-(m+3)}^{n+1} - 2\hat{h}_{j-(m+3)}^{n+1} + \hat{h}_{j-1-(m+3)}^{n+1}}{\Delta\xi^2}\right) & \text{for } j = m+3, \ldots, 2m+3, \\ \frac{1}{6L\Delta\xi}\left(\hat{h}_m^{n+1}\right)^3\left(\hat{p}_{m+1}^{n+1} - \hat{p}_{m-1}^{n+1}\right) - h_0\dot{L}, & \text{for } j = 2m+4. \end{cases}$$

To approximate the second derivative at the boundary (see components E_{m+2}^{n+1} defined by $j = m+2$ and E_{2m+4}^{n+1} defined by $j = 2m+4$), I need one grid point on each side of the boundary. This is why I introduced a ghost point at both boundaries. Thus, I have $2m+6$ variables to solve for. The boundary conditions provide the additional equations in order to have $2m+6$ equations. The flux boundary conditions are implemented at $j = m+2$ and $j = m+4$, and the dirichlet boundary conditions are enforced in components $j = -1$ and $j = m+1$.

At the i-th Newton iteration, the solver is set up to solve $J(\hat{\mathbf{h}}_i, \hat{\mathbf{p}}_i)(< \hat{\mathbf{h}}_i - \hat{\mathbf{h}}^n, \hat{\mathbf{p}}_i - \hat{\mathbf{p}}^n >) = -\mathbf{E}(\hat{\mathbf{h}}_i, \hat{\mathbf{p}}_i)$, where $J \in \mathbb{R}^{(2m+6)\times(2m+6)}$ is the Jacobian of $\mathbf{E}$, and $\hat{\mathbf{h}}_i$ and $\hat{\mathbf{p}}_i$ are the i-th approximation

of the root $< \hat{\mathbf{h}}^{n+1}, \hat{\mathbf{p}}^{n+1} >$. The rows of Jacobian are given by

$$J^{n+1}_{i+1,j+1} = \begin{cases} 1, & \text{for } i = -1, m+1 \text{ and } j = i, \\ \frac{\Delta t}{4L^2\Delta\xi^2}\left(\hat{h}_j^{n+1}\right)^2\left(\hat{p}_{j+1}^{n+1} - \hat{p}_{j-1}^{n+1}\right) + \frac{\Delta t \xi_j \dot{L}}{2\Delta\xi L}, & \text{for } i = 0,\ldots,m \text{ and } j = i-1, \\ 1 - \frac{\Delta t}{2L^2\Delta\xi^2}\hat{h}_j^{n+1}\left(\hat{h}_{j+1}^{n+1} - \hat{h}_{j-1}^{n+1}\right)\left(\hat{p}_{j+1}^{n+1} - \hat{p}_{j-1}^{n+1}\right) & \\ \quad - \frac{\Delta t}{L^2\Delta\xi^2}\left(\hat{h}_j^{n+1}\right)^2\left(\hat{p}_{j+1}^{n+1} - 2\hat{p}_j^{n+1} + \hat{p}_{j-1}^{n+1}\right), & \text{for } i = 0,\ldots,m \text{ and } j = i, \\ -\frac{\Delta t}{4L^2\Delta\xi^2}\left(\hat{h}_j^{n+1}\right)^2\left(\hat{p}_{j+1}^{n+1} - \hat{p}_{j-1}^{n+1}\right) - \frac{\Delta t \xi_j \dot{L}}{2\Delta\xi L}, & \text{for } i = 0,\ldots,m \text{ and } j = i+1, \\ \frac{\Delta t}{4L^2\Delta\xi^2}\left(\hat{h}_j^{n+1}\right)^2\left(\hat{h}_{j+1}^{n+1} - \hat{h}_{j-1}^{n+1}\right) - \frac{\Delta t}{3\Delta\xi^2 L^2}\left(\hat{h}_j^{n+1}\right)^3, & \text{for } i = 0,\ldots,m \text{ and } j = i-1+m+3, \\ \frac{3\Delta t}{2L^2\Delta\xi^2}\left(\hat{h}_j^{n+1}\right)^3, & \text{for } i = 0,\ldots,m \text{ and } j = i+m+3, \\ -\frac{\Delta t}{4L^2\Delta\xi^2}\left(\hat{h}_j^{n+1}\right)^2\left(\hat{h}_{j+1}^{n+1} - \hat{h}_{j-1}^{n+1}\right) - \frac{\Delta t}{3\Delta\xi^2 L^2}\left(\hat{h}_j^{n+1}\right)^3, & \text{for } i = 0,\ldots,m \text{ and } j = i+1+m+3, \\ \frac{S}{L^2\Delta\xi^2}, & \text{for } i = m+3,\ldots,2m+4 \text{ and } j = i-1-(m+3), \\ -\frac{2S}{L^2\Delta\xi^2}, & \text{for } i = m+3,\ldots,2m+4 \text{ and } j = i-(m+3), \\ \frac{S}{L^2\Delta\xi^2}, & \text{for } i = m+3,\ldots,2m+4 \text{ and } j = i+1-(m+3), \\ -\frac{\left(\hat{h}_0^{n+1}\right)^3}{(6L\Delta\xi)}, & \text{for } i = m+2 \text{ and } j = i-1, \\ 1, & \text{for } i = m+4,\ldots,2m+4 \text{ and } j = i, \\ \frac{\left(\hat{h}_m^{n+1}\right)^3}{(6L\Delta\xi)}, & \text{for } i = 2m+4 \text{ and } j = i+1-(m+3), \\ 0, & \text{otherwise} \end{cases}$$

IV. Von Neumann analysis of 1-D model

Prior works have found the approximation of the tear film evolution on a realistic blinking domain to be challenging. The difficulty has been attributed to the fourth derivative scaled by the thickness cubed, the third derivative boundary conditions, and the additional advection term in the mapped equations. These challenges have been overcome by rewriting the fourth-order system as a system of third-order PDEs [12, 20] . In this work, we propose rewriting the PDE as a system of nonlinear second-order PDEs [18, 21]. To gain insight into the numerical behavior, we first linearize the numerical approximation and perform von Neumann analysis on the discretization of both the single PDE and the system of PDEs. In the discretization, as a reminder of notation, $h_j^n \approx h(x_j, t^n)$, where $x_j = j\Delta x$ and $t^n = n\Delta t$, and $\hat{h}_j^n \approx \hat{h}(\xi_j, t^n)$, where $\xi_j = j\Delta\xi$ and $t^n = n\Delta t$. Recall, Δx is the grid spacing in the physical space, $\Delta\xi$ is the grid spacing in the mapped domain, and Δt is the size of the time step.

IV.1 Linear PDE on a fixed domain

The linear PDE that was examined was

$$\frac{\partial h}{\partial t} + S\frac{\partial^4 h}{\partial x^4} = 0. \tag{IV.1}$$

This was discretized as

$$\frac{h_j^{n+1} - h_j^n}{\Delta t} + \frac{S}{(\Delta x)^4}(h_{j+2}^{n+1} - 4h_{j+1}^{n+1} + 6h_j^{n+1} - 4h_{j-1}^{n+1} + h_{j-2}^{n+1}) = 0. \tag{IV.2}$$

In order to examine the stability of this discretization of equation (IV.1), we looked at the effect of the discrete PDE on a plane wave. Let $h_j^n = z^n e^{ikx_j}$ where k is the wave number. Substituting this into equation (IV.2) yields the following:

$$0 = z^{n+1}e^{ikx_j} - z^n e^{ikx_j} + \frac{S\Delta t}{(\Delta x)^4}\left(z^{n+1}e^{ik(x_j+2\Delta x)} - 4z^{n+1}e^{ik(x_j+\Delta x)} + 6z^{n+1}e^{ikx_j} - 4z^{n+1}e^{ik(x_j-\Delta x)} + z^{n+1}e^{ik(x_j-2\Delta x)}\right),$$

$$0 = z^n e^{ikx_j}\left(z - 1 + z\frac{S\Delta t}{(\Delta x)^4}\left(e^{ik2\Delta x} - 4e^{ik\Delta x} + 6 - 4e^{-ik\Delta x} + e^{-ik2\Delta x}\right)\right).$$

If we divide by the nonzero quantity $z^n e^{ikx_j}$ and solve for z we get:

$$0 = z - 1 + z\frac{S\Delta t}{(\Delta x)^4}\left(e^{ik2\Delta x} - 4e^{ik\Delta x} + 6 - 4e^{-ik\Delta x} + e^{-ik2\Delta x}\right),$$

$$1 = z\left(1 + \frac{S\Delta t}{(\Delta x)^4}\left(e^{ik2\Delta x} - 4e^{ik\Delta x} + 6 - 4e^{-ik\Delta x} + e^{-ik2\Delta x}\right)\right),$$

$$z = \frac{1}{1 + \frac{S\Delta t}{(\Delta x)^4}\left(e^{ik2\Delta x} - 4e^{ik\Delta x} + 6 - 4e^{-ik\Delta x} + e^{-ik2\Delta x}\right)}.$$

To better see what is going on, we use Euler's identity to reduce the number of terms

$$z = \frac{1}{1 + \frac{2S\Delta t}{(\Delta x)^4}\left(\cos(k\Delta x) - 4\cos(k\Delta x) + 3\right)}.$$

In order for the scheme to be stable, we need $z \leq 1$. This means that the denominator of z must be greater than or equal to 1. Note that $\frac{2S\Delta t}{(\Delta x)^4}\left(\cos(k\Delta x) - 4\cos(k\Delta x) + 3\right) \geq 0$ regardless of the parameter values of S, Δx, and Δt. Thus the denominator is always at least 1, and consequently z is at most 1. Therefore the code is stable for all parameter values.

IV.2 Linear PDE on moving boundary

The linear mapped PDE that was examined was

$$\frac{\partial \hat{h}}{\partial t} - \frac{\dot{L}\xi}{L}\frac{\partial \hat{h}}{\partial \xi} + \frac{S}{L^4}\frac{\partial^4 \hat{h}}{\partial \xi^4} = 0. \tag{IV.3}$$

Equation (IV.3) was discretized as

$$\frac{\hat{h}_j^{n+1} - \hat{h}_j^n}{\Delta t} - \frac{\dot{L}\xi_j}{2L\Delta\xi}\left(\hat{h}_{j+1}^{n+1} - \hat{h}_{j-1}^{n+1}\right) + \frac{S}{L^4(\Delta\xi)^4}\left(\hat{h}_{j+2}^{n+1} - 4\hat{h}_{j+1}^{n+1} + 6\hat{h}_j^{n+1} - 4\hat{h}_{j-1}^{n+1} + \hat{h}_{j-2}^{n+1}\right) = 0. \tag{IV.4}$$

Let $\hat{h}_j^n = z^n e^{ik\xi_j}$. Substituting this into equation (IV.4) yields

$$\begin{aligned} 0 =& z^{n+1}e^{ik\xi_j} - z^n e^{ik\xi_j} - \frac{\dot{L}\xi_j\Delta t}{2L\Delta\xi}\left(z^{n+1}e^{ik(\xi_j+\Delta\xi)} - z^{n+1}e^{ik(\xi_j-\Delta\xi)}\right) \\ &+ \frac{S\Delta t}{L^4(\Delta\xi)^4}\left(z^{n+1}e^{ik(\xi_j+2\Delta\xi)} - 4z^{n+1}e^{ik(\xi_j+\Delta\xi)} + 6z^{n+1}e^{ik\xi_j} - 4z^{n+1}e^{ik(\xi_j-\Delta\xi)} + z^{n+1}e^{ik(\xi_j+2\Delta\xi)}\right), \end{aligned}$$

$$0 = z^n e^{ik\xi_j}\left(z - 1 - z\frac{\dot{L}\xi_j\Delta t}{2L\Delta\xi}\left(e^{ik\Delta\xi} - e^{-ik\Delta\xi}\right) + z\frac{S\Delta t}{L^4(\Delta\xi)^4}\left(e^{ik2\Delta\xi} - 4e^{ik\Delta\xi} + 6 - 4e^{-ik\Delta\xi} + e^{-ik2\Delta\xi}\right)\right).$$

Dividing by the nonzero term $z^n e^{ik\xi_j}$ and solving for z yields:

$$0 = z - 1 - z\frac{\dot{L}\xi_j\Delta t}{2L\Delta\xi}\left(e^{ik\Delta\xi} - e^{-ik\Delta\xi}\right) + z\frac{S\Delta t}{L^4(\Delta\xi)^4}\left(e^{ik2\Delta\xi} - 4e^{ik\Delta\xi} + 6 - 4e^{-ik\Delta\xi} + e^{-ik2\Delta\xi}\right),$$

$$1 = z\left(1 - \frac{\dot{L}\xi_j\Delta t}{2L\Delta\xi}\left(e^{ik\Delta\xi} - e^{-ik\Delta\xi}\right) + \frac{S\Delta t}{L^4(\Delta\xi)^4}\left(e^{ik2\Delta\xi} - 4e^{ik\Delta\xi} + 6 - 4e^{-ik\Delta\xi} + e^{-ik2\Delta\xi}\right)\right),$$

$$z = \frac{1}{1 - \frac{\dot{L}\xi_j\Delta t}{2L\Delta\xi}\left(e^{ik\Delta\xi} - e^{-ik\Delta\xi}\right) + \frac{S\Delta t}{L^4(\Delta\xi)^4}\left(e^{ik2\Delta\xi} - 4e^{ik\Delta\xi} + 6 - 4e^{-ik\Delta\xi} + e^{-ik2\Delta\xi}\right)}.$$

To better see what is going on, we use Euler's identity to reduce the number of terms

$$z = \frac{1}{1 - \frac{\dot{L}\xi_j\Delta t}{L\Delta\xi} i\sin(k\Delta\xi) + \frac{2S\Delta t}{L^4(\Delta\xi)^4}\left(\cos(k\Delta\xi) - 4\cos(2k\Delta\xi) + 3\right)}.$$

As before, for the scheme to be stable, we need $|z| \leq 1$. This means the magnitude of the denominator must be at least 1:

$$|1 - \frac{\dot{L}\xi_j \Delta t}{L\Delta\xi} i \sin(k\Delta\xi) + \frac{2S\Delta t}{L^4(\Delta\xi)^4} \left(\cos(k\Delta\xi) - 4\cos(2k\Delta\xi) + 3\right)|$$
$$= \sqrt{\left(1 + \frac{2S\Delta t}{L^4(\Delta\xi)^4} \left(\cos(k\Delta\xi) - 4\cos(2k\Delta\xi) + 3\right)\right)^2 + \left(\frac{\dot{L}\xi_j \Delta t}{L\Delta\xi} \sin(k\Delta\xi)\right)^2}.$$

From the previous section, we know that $\left(1 + \frac{2S\Delta t}{L^4(\Delta\xi)^4} \left(\cos(k\Delta\xi) - 4\cos(2k\Delta\xi) + 3\right)\right)^2 \geq 1$. To that we are adding $\left(\frac{\dot{L}\xi_j \Delta t}{L\Delta\xi} \sin(k\Delta\xi)\right)^2$ which is always non-negative. Thus $|z|$ is always at most 1 and the scheme is always stable. The advection term resulting from the lid motion doesn't change the stability of the numerical approximation.

IV.3 Non-linear PDE on moving boundary

The non-linear PDE that was examined was

$$\frac{\partial \hat{h}}{\partial t} - \frac{\dot{L}\xi}{L} \frac{\partial \hat{h}}{\partial \xi} + \frac{S}{L^4} \frac{\partial}{\partial_\xi} \left(\frac{\hat{h}^3}{3} \frac{\partial^3 \hat{h}}{\partial \xi^3}\right) = 0. \tag{IV.5}$$

Equation (IV.5) was discretized as

$$\begin{aligned} 0 =& \frac{\hat{h}_j^{n+1} - \hat{h}_j^n}{\Delta t} - \frac{\dot{L}\xi_j}{2L\Delta\xi} \left(\hat{h}_{j+1}^{n+1} - \hat{h}_{j-1}^{n+1}\right) + \frac{S}{3L^4(\Delta\xi)^4} (\hat{h}_j^{n+1})^3 \left(\hat{h}_{j+2}^{n+1} - 4\hat{h}_{j+1}^{n+1} + 6\hat{h}_j^{n+1} - 4\hat{h}_{j-1}^{n+1} + \hat{h}_{j-2}^{n+1}\right) \\ &+ \frac{S}{2L^4(\Delta\xi)^4} \left(\hat{h}_j^{n+1}\right)^2 \left(\hat{h}_{j+1}^{n+1} - h_{j-1}^{n+1}\right) \left(\frac{1}{2}\hat{h}_{j+2}^{n+1} - \hat{h}_{j+1}^{n+1} + \hat{h}_{j-1}^{n+1} - \frac{1}{2}\hat{h}_{j-2}^{n+1}\right). \end{aligned} \tag{IV.6}$$

In order to use von Neumann analysis to determine the stability of this scheme, we linearized the equation by using the Taylor expansions of $\hat{h}^3$ and $\frac{\partial}{\partial\xi}\hat{h}^3$ around $\xi = 1$. We chose $\xi = 1$ because it corresponds to the upper lid, where the effects of the lid moving ought to be the greatest and thus any instability would likely be found near the upper lid. Note that the tear film thickness is always positive, so $a \approx \hat{h}^3 \geq 0$. Also, the tear film thickness increases as ξ increases near the upper lid, so $b \approx \partial_\xi \hat{h}^3 \geq 0$ near $\xi = 1$.

Using these linear approximations, equation (IV.6) becomes:

$$\begin{aligned} 0 =& \frac{\hat{h}_j^{n+1} - \hat{h}_j^n}{\Delta t} - \frac{\dot{L}\xi_j}{2L\Delta\xi} \left(\hat{h}_{j+1}^{n+1} - \hat{h}_{j-1}^{n+1}\right) + \frac{S}{3L^4(\Delta\xi)^4} a \left(\hat{h}_{j+2}^{n+1} - 4\hat{h}_{j+1}^{n+1} + 6\hat{h}_j^{n+1} - 4\hat{h}_{j-1}^{n+1} + \hat{h}_{j-2}^{n+1}\right) \\ &+ \frac{S}{3L^4(\Delta\xi)^3} b \left(\frac{1}{2}\hat{h}_{j+2}^{n+1} - \hat{h}_{j+1}^{n+1} + \hat{h}_{j-1}^{n+1} - \frac{1}{2}\hat{h}_{j-2}^{n+1}\right). \end{aligned} \tag{IV.7}$$

Now we can use von Neumann analysis like before, and substitute $\hat{h}_j^n = z^n e^{ik\xi_j}$ into equation (IV.7):

$$\begin{aligned}0 =& z^{n+1}e^{ik\xi_j} - z^n e^{ik\xi_j} - \frac{\dot{L}\xi_j\Delta t}{2L\Delta\xi}\left(z^{n+1}e^{ik(\xi_j+\Delta\xi)} - z^{n+1}e^{ik(\xi_j-\Delta\xi)}\right)\\ &+ \frac{aS\Delta t}{3L^4(\Delta\xi)^4}\left(z^{n+1}e^{ik(\xi_j+2\Delta\xi)} - 4z^{n+1}e^{ik(\xi_j+\Delta\xi)} + 6z^{n+1}e^{ik\xi_j} - 4z^{n+1}e^{ik(\xi_j-\Delta\xi)} + z^{n+1}e^{ik(\xi_j-2\Delta\xi)}\right)\\ &+ \frac{bS\Delta t}{3L^4(\Delta\xi)^3}\left(\frac{1}{2}z^{n+1}e^{ik(\xi_j+2\Delta\xi)} - z^{n+1}e^{ik(\xi_j+\Delta\xi)} + z^{n+1}e^{ik(\xi_j-\Delta\xi)} - \frac{1}{2}z^{n+1}e^{ik(\xi_j-2\Delta\xi)}\right),\end{aligned}$$

$$\begin{aligned}0 =& z - 1 - z\frac{\dot{L}\xi_j\Delta t}{2L\Delta\xi}\left(e^{ik\Delta\xi} - e^{-ik\Delta\xi}\right) + z\frac{aS\Delta t}{3L^4(\Delta\xi)^4}\left(e^{2ik\Delta\xi} - 4e^{ik\Delta\xi} + 6 - 4e^{-ik\Delta\xi} + e^{-2ik\Delta\xi}\right)\\ &+ z\frac{bS\Delta t}{3L^4(\Delta\xi)^3}\left(\frac{1}{2}e^{2ik\Delta\xi} - e^{ik\Delta\xi} + e^{-ik\Delta\xi} - \frac{1}{2}e^{-2ik\Delta\xi}\right),\end{aligned}$$

$$\begin{aligned}1 =& z\left(1 - \frac{\dot{L}\xi_j\Delta t}{2L\Delta\xi}\left(e^{ik\Delta\xi} - e^{-ik\Delta\xi}\right) + \frac{aS\Delta t}{3L^4(\Delta\xi)^4}\left(e^{2ik\Delta\xi} - 4e^{ik\Delta\xi} + 6 - 4e^{-ik\Delta\xi} + e^{-2ik\Delta\xi}\right)\right.\\ &\left.+ \frac{bS\Delta t}{3L^4(\Delta\xi)^3}\left(\frac{1}{2}e^{2ik\Delta\xi} - e^{ik\Delta\xi} + e^{-ik\Delta\xi} - \frac{1}{2}e^{-2ik\Delta\xi}\right)\right).\end{aligned}$$

Again, to better see what is going on, we use Euler's identity to simplify the equation:

$$\begin{aligned}1 =& z\left(1 - \frac{\dot{L}\xi_j\Delta t}{2L\Delta\xi}\left(2i\sin(k\Delta\xi)\right) + \frac{aS\Delta t}{3L^4(\Delta\xi)^4}\left(2\cos(2k\Delta\xi) - 8\cos(k\Delta\xi) + 6\right)\right.\\ &\left.+ \frac{bS\Delta t}{3L^4(\Delta\xi)^3}\left(i\sin(2k\Delta\xi) - 2i\sin(k\Delta\xi)\right)\right),\end{aligned}$$

$$1 = z\left(1 - \frac{\dot{L}\xi_j\Delta t}{L\Delta\xi}\left(i\sin(k\Delta\xi)\right) + \frac{2aS\Delta t}{3L^4(\Delta\xi)^4}\left(\cos(k\Delta\xi) - 1\right)^2 + \frac{bS\Delta t}{3L^4(\Delta\xi)^3}\left(i\sin(2k\Delta\xi) - 2i\sin(k\Delta\xi)\right)\right),$$

$$z = \frac{1}{1 - \frac{\dot{L}\xi_j\Delta t}{L\Delta\xi}\left(i\sin(k\Delta\xi)\right) + \frac{2aS\Delta t}{3L^4(\Delta\xi)^4}\left(\cos(k\Delta\xi) - 1\right)^2 + \frac{bS\Delta t}{3L^4(\Delta\xi)^3}\left(i\sin(2k\Delta\xi) - 2i\sin(k\Delta\xi)\right)}. \tag{IV.8}$$

In order for $|z|$ to be at most 1, the magnitude of the denominator of equation (IV.8) must be at least 1:

$$\left|1 - \frac{\dot{L}\xi_j\Delta t}{L\Delta\xi}\left(i\sin(k\Delta\xi)\right) + \frac{2aS\Delta t}{3L^4(\Delta\xi)^4}\left(\cos(k\Delta\xi) - 1\right)^2 + \frac{bS\Delta t}{3L^4(\Delta\xi)^3}\left(i\sin(2k\Delta\xi) - 2i\sin(k\Delta\xi)\right)\right| \geq 1,$$

$$\left|1+\frac{2aS\Delta t}{3L^4(\Delta\xi)^4}\left(\cos(k\Delta\xi)-1\right)^2+i\left(-\frac{\dot{L}\xi_j\Delta t}{L\Delta\xi}\left(\sin(k\Delta\xi)\right)+\frac{bS\Delta t}{3L^4(\Delta\xi)^3}\left(\sin(2k\Delta\xi)-2\sin(k\Delta\xi)\right)\right)\right|\geq 1.$$

This is certainly true, since the real part of the number is always at least one. However, if the assumption that a and b are positive is violated, there is no guarantee that the code is stable. Therefore, at the upper lid, the nonlinearity does not cause instability for physically meaningful values of the tear film thickness and its derivative.

IV.4 Coupled non-linear PDE with moving boundary

The way that the system is solved in Overture is to solve two coupled PDEs. The system is the following:

$$\begin{aligned}\frac{\partial h}{\partial t}-\frac{\partial}{\partial x}\left(\frac{h^3}{3}\frac{\partial p}{\partial x}\right) &= 0,\\ p+S\frac{\partial^2 h}{\partial x^2} &= 0.\end{aligned}$$

After doing the same change of coordinates, the system becomes:

$$\begin{aligned}\frac{\partial \hat{h}}{\partial t}-\frac{\xi\dot{L}}{L}\left(\frac{\partial \hat{h}}{\partial \xi}\right)-\frac{1}{L^2}\frac{\partial}{\partial \xi}\left(\frac{\hat{h}^3}{3}\frac{\partial \hat{p}}{\partial \xi}\right) &= 0,\\ \hat{p}+\frac{S}{L^2}\frac{\partial^2 \hat{h}}{\partial \xi^2} &= 0.\end{aligned}$$

Using the product rule, we get the following:

$$\begin{aligned}\frac{\partial \hat{h}}{\partial t}-\frac{\xi\dot{L}}{L}\left(\frac{\partial \hat{h}}{\partial \xi}\right)-\frac{1}{L^2}\frac{\partial}{\partial \xi}\left(\frac{\hat{h}^3}{3}\right)\frac{\partial \hat{p}}{\partial \xi}-\frac{1}{L^2}\frac{\hat{h}^3}{3}\frac{\partial^2 \hat{p}}{\partial \xi^2} &= 0,\\ \hat{p}+\frac{S}{L^2}\frac{\partial^2 \hat{h}}{\partial \xi^2} &= 0.\end{aligned}$$

To linearize this, we let a equal the Taylor series expansion of $\frac{\hat{h}^3}{3}$ and b equal the Taylor series expansion of $\frac{\partial}{\partial \xi}\frac{\hat{h}^3}{3}$. Then the system becomes:

$$\begin{aligned}\frac{\partial \hat{h}}{\partial t}-\frac{\xi\dot{L}}{L}\left(\frac{\partial \hat{h}}{\partial \xi}\right)-\frac{b}{L^2}\frac{\partial \hat{p}}{\partial \xi}-\frac{a}{L^2}\frac{\partial^2 \hat{p}}{\partial \xi^2} &= 0,\\ \hat{p}+\frac{S}{L^2}\frac{\partial^2 \hat{h}}{\partial \xi^2} &= 0.\end{aligned}$$

Discretized, this becomes:

$$\begin{aligned}\frac{\hat{h}_j^{n+1}-\hat{h}_j^n}{\Delta t}-\frac{\xi_j\dot{L}}{2L\Delta\xi}\left(\hat{h}_{j+1}^{n+1}-\hat{h}_{j-1}^{n+1}\right)-\frac{b}{2L^2\Delta\xi}\left(\hat{p}_{j+1}^{n+1}-\hat{p}_{j-1}^{n+1}\right)-\frac{a}{L^2\Delta\xi^2}\left(\hat{p}_{j+1}^{n+1}-2\hat{p}_j^{n+1}+\hat{p}_{j-1}^{n+1}\right) &= 0,\\ \hat{p}_j^{n+1}+\frac{S}{L^2\Delta\xi^2}\left(\hat{h}_{j+1}^{n+1}-2\hat{h}_j^{n+1}+\hat{h}_{j-1}^{n+1}\right) &= 0.\end{aligned}$$

This can be written as the following matrix equation:

$$\begin{bmatrix}1&0\\0&0\end{bmatrix}\begin{bmatrix}\hat{h}_j^n\\\hat{p}_j^n\end{bmatrix}=\begin{bmatrix}-\frac{\xi_j\dot{L}\Delta t}{2L\Delta\xi}&\frac{-b\Delta t}{2L^2\Delta\xi}-\frac{a\Delta t}{L\Delta\xi^2}\\\frac{S}{L^2\Delta\xi^2}&0\end{bmatrix}\begin{bmatrix}\hat{h}_{j+1}^{n+1}\\\hat{p}_{j+1}^{n+1}\end{bmatrix}+\begin{bmatrix}1&\frac{2a\Delta t}{L^2\Delta\xi^2}\\\frac{-2S}{L^2\Delta\xi^2}&1\end{bmatrix}\begin{bmatrix}\hat{h}_j^{n+1}\\\hat{p}_j^{n+1}\end{bmatrix}+\begin{bmatrix}\frac{\xi_j\dot{L}\Delta t}{2L\Delta\xi}&\frac{b\Delta t}{2L^2\Delta\xi}-\frac{a\Delta t}{L^2\Delta\xi^2}\\\frac{S}{L^2\Delta\xi^2}&0\end{bmatrix}\begin{bmatrix}\hat{h}_{j-1}^{n+1}\\\hat{p}_{j-1}^{n+1}\end{bmatrix} \tag{IV.9}$$

To do the von Neumann analysis in this 2-D case, we use the discrete Fourier transform, denoted $\mathcal{F}\{\}$. To do this, we will think of matrix equation (IV.9) as a convolution between a sequence of matrices and a sequence of vectors of the form $\beta * \mathbf{w}^n = \alpha * \mathbf{w}^{n+1}$. Due to the convolution theorem, we know that the Fourier transform of a convolution, $\mathcal{F}\{\beta * \mathbf{w}^n\} = \mathcal{F}\{\alpha * \mathbf{w}^{n+1}\}$, is just the product of the Fourier transforms, so our equation can be written in the form $\mathcal{F}\{\beta\}\mathcal{F}\{\mathbf{w}^n\} = \mathcal{F}\{\alpha\}\mathcal{F}\{\mathbf{w}^{n+1}\}$. If $\mathcal{F}\{\alpha\}$ is invertible, then we have the equation $\mathcal{F}\{\mathbf{w}^{n+1}\} = \mathcal{F}\{\alpha\}^{-1}\mathcal{F}\{\beta\}\mathcal{F}\{\mathbf{w}^n\}$. The amplification matrix is then $A = \mathcal{F}\{\alpha\}^{-1}\mathcal{F}\{\beta\}$. If the eigenvalues of the amplification matrix are both less than 1, then the numerical scheme is stable. First, I find $\mathcal{F}\{\beta\}$. By definition,

$$(\beta * \mathbf{w}^n)_p = \sum_{j=-\infty}^{\infty} \Delta\xi \beta_{p-j} w_j^n.$$

In order for this to get the desired product in matrix equation (IV.9), let $\beta_p = \begin{bmatrix}\frac{1}{\Delta\xi}&0\\0&0\end{bmatrix}$. Then:

$$\mathcal{F}\{\beta\} = e^{-ikj\Delta\xi}\begin{bmatrix}1&0\\0&0\end{bmatrix}$$

Next, I find $\mathcal{F}\{\alpha\}$. By definition,

$$(\alpha * \mathbf{w}^{n+1})_p = \sum_{j=-\infty}^{\infty} \Delta\xi \alpha_{p-j} w_j^{n+1}.$$

In order for this to get the desired product in matrix equation (IV.9), we multiply the matrices by

$\frac{1}{\Delta\xi}$ so that we get:

$$\alpha_{j-1} = \frac{1}{\Delta\xi}\begin{bmatrix} \frac{\xi_j \dot{L}\Delta t}{2L\Delta\xi} & \frac{b\Delta t}{2L^2\Delta\xi} - \frac{a\Delta t}{L^2\Delta\xi^2} \\ \frac{S}{L^2\Delta\xi^2} & 0 \end{bmatrix}$$

$$\alpha_j = \frac{1}{\Delta\xi}\begin{bmatrix} 1 & \frac{2a\Delta t}{L^2\Delta\xi^2} \\ \frac{-2S}{L^2\Delta\xi^2} & 1 \end{bmatrix}$$

$$\alpha_{j+1} = \frac{1}{\Delta\xi}\begin{bmatrix} -\frac{\xi_j \dot{L}\Delta t}{2L\Delta\xi} & \frac{-b\Delta t}{2L^2\Delta\xi} - \frac{a\Delta t}{L\Delta\xi^2} \\ \frac{S}{L^2\Delta\xi^2} & 0 \end{bmatrix}$$

Then, $\mathcal{F}\{\alpha\} = \sum_{j=-\infty}^{\infty} \Delta\xi \alpha_j e^{-ikj\Delta\xi}$ gets us:

$$\begin{aligned}
\mathcal{F}\{\alpha\} &= e^{-ik(j-1)\Delta\xi}\begin{bmatrix} \frac{\xi_j \dot{L}\Delta t}{2L\Delta\xi} & \frac{b\Delta t}{2L^2\Delta\xi} - \frac{a\Delta t}{L\Delta\xi^2} \\ \frac{S}{L^2\Delta\xi^2} & 0 \end{bmatrix} + e^{-ikj\Delta\xi_j}\begin{bmatrix} 1 & \frac{2a\Delta t}{L\Delta\xi^2} \\ \frac{-2S}{L^2\Delta\xi^2} & 1 \end{bmatrix} + e^{-ik(j+1)\Delta\xi}\begin{bmatrix} -\frac{\xi_j \dot{L}\Delta t}{2L\Delta\xi} & \frac{-b\Delta t}{2L^2\Delta\xi} - \frac{a\Delta t}{L\Delta\xi^2} \\ \frac{S}{L^2\Delta\xi^2} & 0 \end{bmatrix} \\
&= e^{-ikj\Delta\xi}\begin{bmatrix} e^{ik\Delta\xi}\frac{\xi_j \dot{L}\Delta t}{2L\Delta\xi} + 1 - e^{-ik\Delta\xi}\frac{\xi_j \dot{L}\Delta t}{2L\Delta\xi} & e^{ik\Delta\xi}\left(\frac{b\Delta t}{2L^2\Delta\xi} - \frac{a\Delta t}{L\Delta\xi^2}\right) + \frac{2a\Delta t}{L\Delta\xi^2} + e^{-ik\Delta\xi}\left(-\frac{b\Delta t}{2L^2\Delta\xi} - \frac{a\Delta t}{L\Delta\xi^2}\right) \\ e^{ik\Delta\xi}\frac{S}{L^2\Delta\xi^2} - \frac{2S}{L^2\Delta\xi^2} + e^{-ik\Delta\xi}\frac{S}{L^2\Delta\xi^2} & 1 \end{bmatrix} \\
&= e^{-ikj\Delta\xi}\begin{bmatrix} \frac{\xi_j \dot{L}\Delta t}{L\Delta\xi} i\sin(k\Delta\xi) + 1 & \frac{b\Delta t}{L^2\Delta\xi} i\sin(k\Delta\xi) - \frac{2a\Delta t}{L\Delta\xi^2}\cos(k\Delta\xi) + \frac{2a\Delta t}{L\Delta\xi^2} \\ \frac{2S}{L^2\Delta\xi^2}\cos(k\Delta\xi) - \frac{2S}{L^2\Delta\xi^2} & 1 \end{bmatrix}
\end{aligned}$$

For $\mathcal{F}\{\alpha\}$ to be invertible, we need $\det(\mathcal{F}\{\alpha\}) \neq 0$.

$$\begin{aligned}
\det(\mathcal{F}\{\alpha\}) &= \frac{\xi_j \dot{L}\Delta t}{L\Delta\xi} i\sin(k\Delta\xi) + 1 - \left(\frac{b\Delta t}{L^2\Delta\xi} i\sin(k\Delta\xi) - \frac{2a\Delta t}{L\Delta\xi^2}\cos(k\Delta\xi) + \frac{2a\Delta t}{L\Delta\xi^2}\right)\left(\frac{2S}{L^2\Delta\xi^2}\cos(k\Delta\xi) - \frac{2S}{L^2\Delta\xi^2}\right) \\
&= 1 + \frac{4aS\Delta t}{L^3\Delta\xi^4}(1 - \cos(k\Delta\xi))^2 + i\sin(k\Delta\xi)\left(\frac{2bS\Delta t}{L^4\Delta\xi^3} + \frac{\xi_j \dot{L}\Delta t}{L\Delta\xi} - \frac{2bS\Delta t}{L^4\Delta\xi^3}\cos(k\Delta\xi)\right)
\end{aligned}$$

Notice that if $\det(\mathcal{F}\{\alpha\}) = 0$, then both the real and imaginary parts must be zero simultaneously. However, the piece contributed by the real part of the determinant is never zero. Thus, $\mathcal{F}\{\alpha\}$ is always invertible.

$$\mathcal{F}\{\alpha\}^{-1} = \frac{1}{det(\mathcal{F}\{\alpha\})}\begin{bmatrix} 1 & -\frac{b\Delta t}{L^2\Delta\xi} i\sin(k\Delta\xi) + \frac{2a\Delta t}{L\Delta\xi^2}\cos(k\Delta\xi) - \frac{2a\Delta t}{L\Delta\xi^2} \\ -\frac{2S}{L^2\Delta\xi^2}\cos(k\Delta\xi) + \frac{2S}{L^2\Delta\xi^2} & \frac{\xi_j \dot{L}\Delta t}{L\Delta\xi} i\sin(k\Delta\xi) + 1 \end{bmatrix}$$

Now, we can see that the amplification matrix $A = \mathcal{F}\{\alpha\}^{-1}\mathcal{F}\{\beta\}$ is:

$$A = \frac{1}{\det(\mathcal{F}\{\alpha\})}\begin{bmatrix} 1 & -\frac{b\Delta t}{L^2\Delta\xi}i\sin(k\Delta\xi) + \frac{2a\Delta t}{L\Delta\xi^2}\cos(k\Delta\xi) - \frac{2a\Delta t}{L\Delta\xi^2} \\ -\frac{2S}{L^2\Delta\xi^2}\cos(k\Delta\xi) + \frac{2S}{L^2\Delta\xi^2} & \frac{\xi_j\dot{L}\Delta t}{L\Delta\xi}i\sin(k\Delta\xi) + 1 \end{bmatrix}\begin{bmatrix} 1 & 0 \\ 0 & 0 \end{bmatrix}$$
$$= \frac{1}{\det(\mathcal{F}\{\alpha\})}\begin{bmatrix} 1 & 0 \\ -\frac{2S}{L^2\Delta\xi^2}\cos(k\Delta\xi) + \frac{2S}{L^2\Delta\xi^2} & 0 \end{bmatrix}$$

Now, I examine the eigenvalues of A.

$$\begin{cases} \lambda_1 = 0 \\ \lambda_2 = \frac{1}{1+\frac{4aS\Delta t}{L^3\Delta\xi^4}(1-\cos(k\Delta\xi))^2 + i\sin(k\Delta\xi)\left(\frac{2bS\Delta t}{L^4\Delta\xi^3} + \frac{\xi_j\dot{L}\Delta t}{L\Delta\xi} - \frac{2bS\Delta t}{L^4\Delta\xi^3}\cos(k\Delta\xi)\right)}. \end{cases}$$

Clearly, $|\lambda_1| \leq 1$. Note that the denominator of $|\lambda_2|$ is always at least 1 since the real part is always at least one. Thus $|\lambda_2|$ is at most one. Therefore the scheme is stable for all parameter values. However, as in the previous section, if a or b are negative, the algorithm may not be stable.

In general, I found the numerical algorithm for the two different mapped systems to be stable for all parameter values and physically meaningful values of a and b. In the next section, I explore the conditioning of each numerical formulation and study how the choice of boundary conditions influence the behavior of the numerical algorithm.

V. Validation and verification

In order to validate that the codes converge, and verify that they conserve volume, simulations were run with both the single PDE and PDE system codes for the three lid functions on four different grids. The tear film thickness and pressure vectors were recorded every 1000 time steps for analysis. As found in the literature, the mapped single PDE is challenging to numerically approximate. I was unable to solve the single PDE with any of the third derivative (flux) boundary conditions with my Newton solver for a wide range of parameter values. The condition number of the Jacobian grows out of control within the first time step. The Jacobian is better conditioned when using Boundary Condition 3, however the condition number still grows above 10^{10} within the first time step. Moving forward, I consider just the couple PDE system.

V.1 Convergence

The mapped coupled PDE system (also referred to as the “pressure code") was then tested with each of the three lid functions, to confirm that as the grid is refined, the relative computational error decreases. I compared the coarser grids to the most refined grid to find the relative error in the tear film thickness. The model was discretized second-order in space, so the error should reduce quadratically. I used the largest Δt the code could accommodate; that is, Newton solver at each time step would converge in a couple of steps. Results from over the course of a blink which were recorded every 1000 time steps were used to calculate the rate of convergence. Table 2 shows the values.

lid function	Δt	$\Delta\xi$	thickness max relative error
Trig	10^{-5}	.01	0.9894
		.005	0.1839
		.0025	0.0350
Aydemir	10^{-4}	.01	0.9469
		.005	0.1794
		.0025	0.0343
Realistic	5×10^{-5}	.01	0.6534
		.005	0.1312
		.0025	0.0253

Table 2: The maximum relative error of the tear film thickness. The relative error was found by comparing the solution on coarse and fine grids.

To determine the rate of convergence, I fit a line to log(max error) vs $\log(\Delta\xi)$. The slope for this line when using the trig lid function was 2.41, when using the Aydemir lid function was 2.39, and lastly when using the realistic blink was 2.35. This is consistent with the PDEs being discretized second-order in space.

V.2 Conservation of volume

Then, the pressure code was tested with each of the three lid functions to confirm that the tear film volume is truly conserved as was imposed by the boundary conditions. I compute the relative error of the volume compared to the initial volume. This is done every 1000 time steps. In table

(3). The maximum relative error of the volume is recorded as above, every 1000 time steps over the course of a blink.

lid function	Δt	$\Delta\xi$	volume max relative error
Trig	10^{-5}	.01	0.0377
		.005	0.0079
		.0025	0.0019
		.00125	0.0005
Aydemir	10^{-4}	.01	0.0374
		.005	0.0079
		.0025	0.0019
		.00125	0.005
Realistic	5×10^{-5}	.01	0.1440
		.005	0.1674
		.0025	0.1727
		.00125	0.1714

Table 3: The maximum relative error of the tear film volume over a blink for the different lid functions.

As the maximum relative error of the tear film volume is small, shown in Table 3, the code does conserve the tear fluid over the course of the blink as imposed by the flux boundary conditions.

VI. Results

Various parameter combinations were used to explore the behavior of this system. An example result is shown below in Figures 6 and 7. These results are from a grid spacing of $\Delta\xi = .0025$, $\Delta t = 10^{-4}$, $S = 10^{-6}$, $h_0 = 13$, with boundary condition 1, and using the Aydemir lid function. We can see that as the eye opens, the tear film thins in the center of the open eye, but at the lids the thickness is fixed at 13. The tear film must thin as more eye surface is exposed as the flux boundary conditions enforce conservation of volume. While the eye opens there is a gradual decrease in thickness between the upper lid and the center of the eye that makes way for the minimum next to the upper lid that becomes more apparent while the eye closes. This is consistent with the existence of the tear film meniscus at the lids, and the adjacent black line thinning next to the lid. While the eye closes, the pressure profile looks quite different from when it opens. This is due to the meniscus drawing the tear film toward the upper lid while the lid tries to push the fluid in the opposite direction.

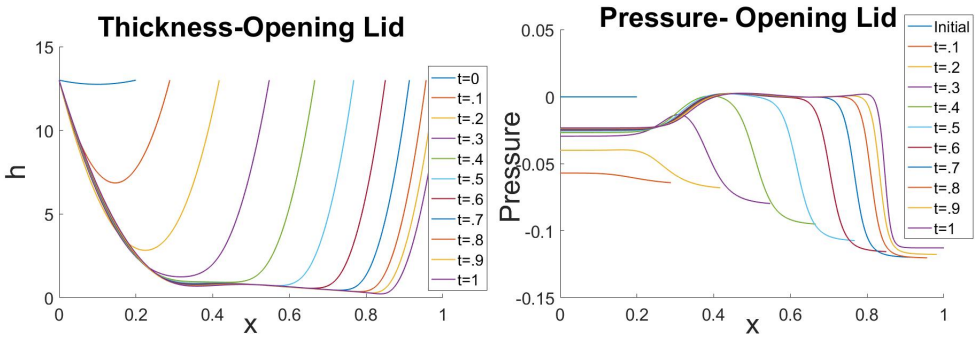

Figure 6: The tear film thickness and pressure profiles while the eye opens.

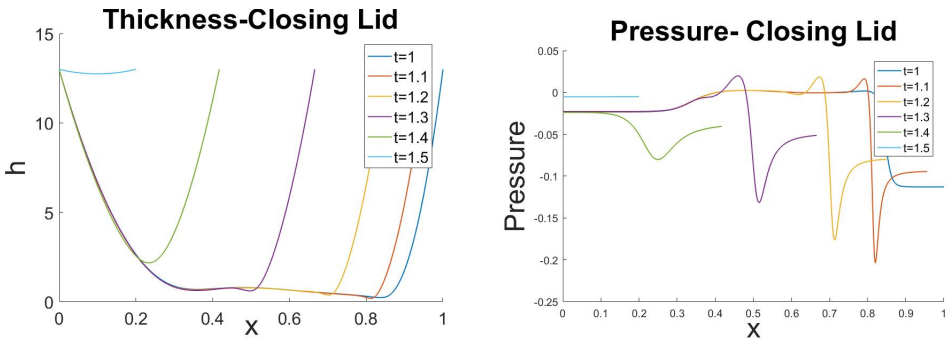

Figure 7: The tear film thickness and pressure profiles while the eye closes.

VI.1 Comparison with other boundary conditions

As the boundary conditions severely influenced the behavior of the mapped single PDE, I analyzed how the three boundary conditions affect the conditioning of the Jacobian and the time it takes to compute the solution. I compare code performance for each of these boundary conditions. This was done on a grid spacing of $\Delta\xi = .005$, $S = 10^{-6}$, $h_0 = 13$ and $\Delta t = .5 \times 10^{-4}$.

Lid	Boundary Conditions	$\max(\kappa(J))$	$\text{avg}(\kappa(J))$	time (s)
Trig	1	2.1×10^7	3.6×10^6	831
Trig	2	1.2×10^7	6.0×10^6	1104
Trig	3	9×10^{10}	5.3×10^9	1657
Aydemir	1	1.8×10^8	3.0×10^6	833
Aydemir	2	1.7×10^7	5.0×10^6	1105
Aydemir	3	3.4×10^{10}	2.1×10^9	1499
Realistic	1	5.5×10^8	3.0×10^6	2317
Realistic	2	1.5×10^7	5.8×10^6	1265
Realistic	3	6.1×10^{10}	2.5×10^9	1664

The condition number, $\kappa(J)$, is the highest as the eye begins to open and when the eye is almost closed. The condition number is comparatively low for the main portion of the blink. Using an adaptive time step, where Δt is smaller when the eye is transitioning from closing to opening, may improve the conditioning of the Jacobian at those times. Also note that the condition number is consistently much higher for boundary condition 3. This suggests that the pressure at the upper lid needs to change over time.

VI.2 Comparison with 2-D simulation

Just how much does the tear fluid's ability to spread sideways on the 2-D eye matter? Does this ability effectively lower pressure gradients and meaningfully change the thickness profile? To answer these questions, we compared results from my code to two dimensional results from Overture for the same parameters, boundary conditions, and initial conditions. The results in Overture were on a variable grid with average spacing 0.005, so I used $\Delta\xi = .005$. I let $\Delta t = 5 \times 10^{-5}, S = 7.86 \times 10^{-7}, h_0 = 13$. Figure (8) shows results from the upstroke, while Figure (9) shows results from the downstroke.

The one-dimensional results show the same behavior as the two-dimensional results qualitatively,

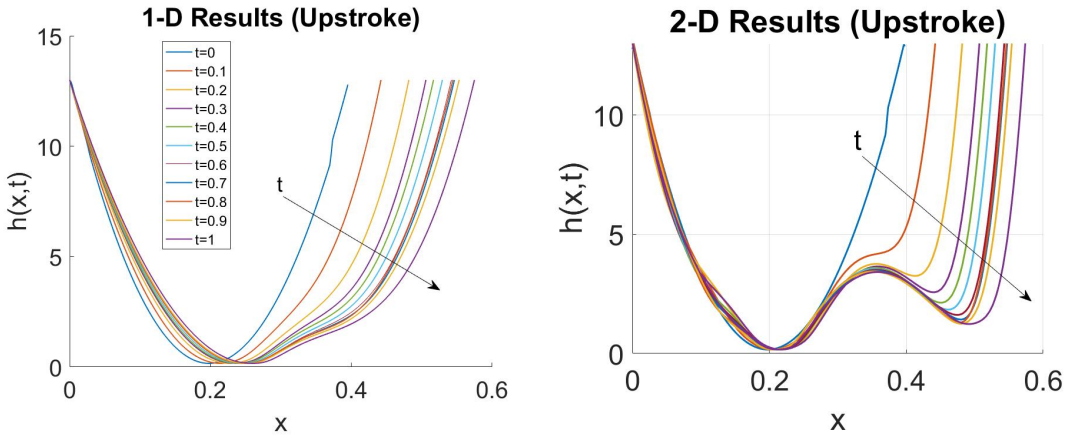

Figure 8: Comparison of results between the 1-D and 2-D simulations during the upstroke.

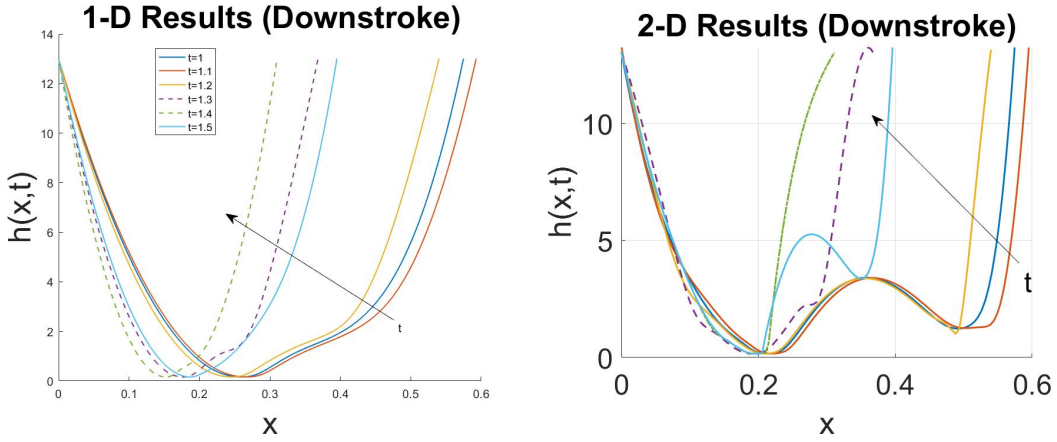

Figure 9: Comparison of results between the 1-D and 2-D simulations during the upstroke.

but to a much lesser degree. Notice that the black line at the upper lid around $x = 0.5$ is much more pronounced in the two-dimensional results. Clearly, the pressure gradients are greater in the two-dimensional results. In two dimensions, it appears that the tear film can move around more which makes sense since it can have more curvature in another dimension thus driving additional flow into the meniscus.

VII. Conclusion

The numerical approximation of the one-dimensional model is stable for all parameter values, which suggests that the similar two dimensional model ought to also be stable. There is no loss or gain of stability from the alternate formulation. However, the von Neumann analysis did not

take the boundary conditions into consideration, so while the finite difference approximation of the PDE itself is stable, the choice of boundary condition may generate a poorly conditioned problem.

The problem is due to poor conditioning of the Jacobian matrix and the Newton solver being unable to find a solution within the given tolerance. Specifically, as the upper lid is about to start closing, the Newton's solver cannot find a solution for the next time step, and the Jacobian gets poorly defined when the eye is nearly closed. These are the when the lid velocity is transitioning from zero to negative or vice versa. The step size in both space and time must be small enough for the Jacobian to be well conditioned and the Newton solver to be able to find the next step. Decreasing the time step does improve the condition number of the Jacobian. Additionally, the Jacobian of the coupled PDE system is sensitive to the choice of boundary condition.

The one-dimensional results from my code are consistent with the results from Overture, but do not display the hallmark characteristics of the tear film to the same degree. The tear fluid does seem constrained by only having one dimension.

Based on these results, I conclude that formulating the model as the coupled system in thickness and pressure, as done in Overture, is indeed advantageous for approximating the tear film profile over time. I would recommend using an adaptive time step where Δt is smallest near where the lid is most closed and most open, as that is where my code would usually fail. Additionally, I would recommend formulating the boundary conditions with the variable thickness at the boundary rather than the parameter h_0 as this improved the conditioning of the Jacobian.

With this information, researchers can be better informed and thus save computational time when developing and running further simulations. In the future, similar work could be done on a more involved model that includes the effects of things such as gravity, osmosis, and body temperature. There is still a lot to learn about the tear film behaves in order to determine causes, best treatments, and hopefully cures for dry eye syndrome.

VIII. Acknowledgments

I would first like to thank Dr. Maki for her time and effort, teaching me and helping me learn about computational fluid dynamics. I would also like to thank Dr. Li for all of his software assistance. Lastly, I would like to thank my committee for their time and feedback.

The material is based upon work supported by the National Science Foundation under Award No. DMS-1412141.

References

[1] E. Aydemir, C.J. W. Breward, and T.P. Witelski. The effect of polar lipids on tear film dynamics. *Bull. Math. Biol.*, 73(6):1171–1201, 2011.

[2] R.R. Berger and S. Corrsin. A surface tension gradient mechanism for driving the pre-corneal tear film after a blink. *J. Biomech.*, 7:225–238, 1974.

[3] R.J. Braun. Dynamics of the tear film. *Annual Review of Fluid Mechanics.*, 44:267–297, 2012.

[4] R.J. Braun and P.E. King-Smith. Model problems for the tear film in a blink cycle: single-equation models. *J. Fluid Mech.*, 586:465–490, 2007.

[5] A.J. Bron, J.M. Tiffany, S.M. Gouvenia, N. Yokoi, and L.W. Voon. Functional aspects of the tear film lipid layer. *Experimental Eye Research*, 78(3):347–360, 2004.

[6] J.P. Craig, *et. al*. TFOS DEWS II report executive summary. *The Ocular Surface*, 1(11), 2017.

[7] D.A. Dartt, R.R. Hodges, and D. Zoukhri. Tears and their secretion. *Advances in Organ Biology*, 10:21–82, 2005.

[8] M.G. Doane. Interaction of eyelids and tears in corneal wetting and the dynamics of the normal human eyeblink. *Am. J. Ophthalmol.*, 89:507–516, 1980.

[9] I.K. Gibson. Distribution of mucins at the ocular surface. *Experimental Eye Research*, 78(3):379–388, 2004.

[10] I.K. Gipson and T. Inatomi. Mucin genes expressed by the ocular surface epithelium. *Progress in Retinal and Eye Research*, 16(1):81–98, 1992.

[11] T.R. Golding, A.S. Bruce, and J.C. Mainstone. Relationship between tear-meniscus parameters and tear-film breakup. *Cornea*, 16:649–661, 1997.

[12] A. Heryudono, R.J. Braun, T.A. Driscoll, K.L. Maki, L.P. Cook, and P.E. King-Smith. Single-equation models for the tear film in a blink cycle: realistic lid motion. *Mathematical Medicine and Biology: A Journal of the IMA*, 24(4):347–377, 2007.

[13] F.J. Holly. Formation and rupture of the tear film. *Experimental Eye Research*, 15:515–525, 1973.

[14] M.E. Johnson and P.J. Murphy. Changes in the tear film and ocular surface from dry eye syndrome. *Prog. Retin. Eye Res.*, 23(4):449–474.

[15] M.B. Jones, G.R. Fulford, C.P. Please, D.L.S. McElwain, and M.J. Collins. Elastohydrodynamics of the eyelid wiper. *Bull. Math. Biol.*, 70(2):323–343, 2008.

[16] P.E. King-Smith, B.A. Fink, K.K. Nichols, R.M. Hill, and G.S. Wilson. The thickness of the human precorneal tear film: evidence from reflection spectra. *Investig. Opthalmol. Vis. Sci.*, 41(11):3348–3359, 2000.

[17] P.E. King-Smith, K.S. Reuter, R.J. Braun, J.J. Nichols, and K.K. Nichols. Tear film breakup and structure studied by simultaneous video recording of fluorescence and tear film lipid layer images. *Investigative Ophthalmology & Visual Science*, 54(7):4900, 2013.

[18] L. Li, R.J. Braun, K.L. Maki, W.D. Henshaw, and P.E. King-Smith. Tear film dynamics with evaporation, wetting, and time-dependent flux boundary condition on an eye-shaped domain. *Physics of Fluids*, 26:1–24, 2014.

[19] E.A. MacDonald and D.M. Maurice. The kinetics of tear fluid under the lower lid. *Exp. Eye Res.*, 53(4):421–425, 1991.

[20] K.L. Maki, R. J. Braun, T.A. Driscoll, and P.E. King-Smith. An overset grid method for the study of reflex tearing. *Mathematical Medicine and Biology: A Journal of the IMA*, 25(3):187–214, 2008.

[21] K.L. Maki, R.J. Braun, P. Ucciferro, W. D. Henshaw, and P.E. King-Smith. Tear film dynamics on an eye-shaped domain. II. Flux boundary conditions. *J. Fluid Mech.*, 647:361–390, 2010.

[22] S. Mishima, A. Gasset, S.D. Klyce Jr, and J.L. Baum. Determination of tear volume and tear flow. *Investigational Opthalmologoy*, 5(3):264–276, 1996.

[23] R. Robert Montés-Micó, A. Alejandro Cervino, T. Ferrer-Blasco, S. Garía-Lázaro, and D. Madrid-Costa. The tear film and the optical quality of the eye. *The Optical Surface*, 8(4):185 – 192, 2010.

[24] H. Wong, I. Fatt, and C.J. Radke. Deposition and thinning of the human tear film. *Journal of Colloid and Interface Science*, 184(0595):44–51, 1996.